



Did Late Cretaceous cooling trigger the Campanian–Maastrichtian Boundary Event?

Christian Linnert^{1,2*}, Stuart A. Robinson³, Jackie A. Lees¹,
Irene Pérez-Rodríguez⁴, Hugh C. Jenkyns³, Maria Rose Petrizzo⁵,
José A. Arz⁴, Paul R. Bown¹, and Francesca Falzoni⁵

With 6 figures

Abstract. The Campanian–Maastrichtian (83–66 Ma) was a period of global climate cooling, featuring significant negative carbon-isotope ($\delta^{13}\text{C}$) anomalies, such as the Late Campanian Event (LCE) and the Campanian–Maastrichtian Boundary Event (CMBE). A variety of factors, including changes in temperature, oceanic circulation and gateway opening, have been invoked to explain these $\delta^{13}\text{C}$ perturbations, but no precise mechanism has yet been well constrained. In order to improve our understanding of these events, we measured stable carbon and oxygen isotopes of hemipelagic sediments from the Shuqualak-Evans cored borehole (Mississippi, USA) and compared the data with previously published sea-surface temperature (SST) estimates from the same core. We found that the CMBE can be recognised, unambiguously, in the Shuqualak-Evans core, and that it is associated with an interval of cooler SSTs suggesting a possible mechanistic link between palaeotemperature change and this event. Determining the precise position of the LCE in the Shuqualak-Evans core is more problematic, but it may also be associated with cooler SSTs. Our combined records of carbon cycling and SSTs compare well with other studies and provide evidence that cooling during the CMBE (and possibly LCE) was global in nature and affected surface waters, in addition to the deep-ocean. We suggest that short-term cooling drove intensification of high-latitude deep-water formation, which in turn led to changes in the ratio of carbonate to organic carbon burial that led to a negative $\delta^{13}\text{C}$ excursion. Critically, the absence of warming during these intervals implies that the Late Cretaceous events must not have been associated with an appreciable increase in atmospheric $p\text{CO}_2$, and was likely associated with decreased $p\text{CO}_2$.

Key words. Latest Cretaceous cooling, carbon isotope excursions, Late Campanian Event, Campanian–Maastrichtian Boundary Event

Authors' addresses:

¹ Department of Earth Sciences, University College London, Gower Street, London, WC1E 6BT, UK.

² Ruhr-Universität Bochum, Fakultät für Geowissenschaften, Institut für Geologie, Mineralogie und Geophysik, Universitätsstr. 150, 44780 Bochum, Germany.

³ Department of Earth Sciences, University of Oxford, South Parks Road, Oxford, OX1 3AN, UK.

⁴ Departamento de Ciencias de la Tierra, Instituto de Investigación en Ciencias Ambientales (IUCA), Universidad de Zaragoza, Pedro Cerbuna, 12, E-50009 Zaragoza, Spain.

⁵ Dipartimento di Scienzedella Terra “A. Desio”, Università degli Studi di Milano, via Mangiagalli 34, 20133 Milano, Italy.

* Corresponding author: Christian.Linnert@ruhr-uni-bochum.de

1. Introduction

The early Late Cretaceous (Cenomanian–Turonian) was characterised by one of the warmest palaeoclimates of the past 140 million years ('hothouse climate': Wilson et al. 2002, Hay 2008, 2011, Friedrich et al. 2012, Kidder and Worsley 2012, MacLeod et al. 2013). This Cenomanian–Turonian world likely featured ice-free polar regions (Barron et al. 1981, Barron 1983, Ladant and Donnadiou 2016), tropical and subtropical sea-surface temperatures (SSTs) warmer than 35°C (Forster et al. 2007, Bornemann et al. 2008, Sinninghe Damsté et al. 2010, MacLeod et al. 2013) and a shallow latitudinal temperature gradient (Huber et al. 1995, 2002, Bice et al. 2003, Hay and Floegel 2012). By contrast, the late Turonian–Maastrichtian is considered an interval of global cooling (e.g., Clarke and Jenkyns 1999, Linnert et al. 2014), possibly driven by declining atmospheric $p\text{CO}_2$ (e.g., Jenkyns et al. 1994, Berner and Kothavala 2001, Tabor et al. 2016). This decrease in $p\text{CO}_2$ may have been the result of reduced rates of mid-ocean ridge and large igneous province activity (Larson 1991, Coffin et al. 2006). Additionally, the reconfiguration of oceanic gateways may have affected deep-water circulation and oceanic heat transport. For example, it has been suggested that opening of the Equatorial Atlantic Seaway contributed to Late Cretaceous cooling by allowing cool southern-component waters to enter the warm North Atlantic Basin (e.g. Frank and Arthur 1999, Friedrich et al. 2012).

The Campanian is a key interval in the Late Cretaceous, as it marks the transition between the mid-Cretaceous 'hot greenhouse' and the 'cool greenhouse' of the Maastrichtian and early Paleocene (Clarke and Jenkyns 1999, Zachos et al. 2008, Friedrich et al. 2012, Ando et al. 2013, Linnert et al. 2014, Falzoni et al. 2016). The cooling was accompanied by changes in global oceanic circulation towards a mode of deep-water formation in high southern latitudes, although the precise timing and geographic influence of these changes is still being revealed (Barrera and Savin 1999, Frank and Arthur 1999, Huber et al. 2002, Cramer et al. 2009, Robinson et al. 2010, MacLeod et al. 2011, Friedrich et al. 2012, Martin et al. 2012, Robinson and Vance 2012, Murphy and Thomas 2012, 2013, Jung et al. 2013, Voigt et al. 2013, Moiroud et al. 2013, 2016, Donnadiou et al. 2016). Changes in the location and style of deep-water formation have been considered as possible triggers for perturbations of the global carbon cycle, such as the Campanian–

Maastrichtian Boundary Event (CMBE; Friedrich et al. 2009). However, other factors, such as eustatic sea-level falls (Jarvis et al. 2002, 2006), a reduced rate of organic-matter flux (Friedrich et al. 2009) and tectonic processes (Voigt et al. 2010, 2012) may also have contributed.

Here, we present new Campanian–Maastrichtian bulk-rock geochemical data ($\delta^{13}\text{C}$, $\delta^{18}\text{O}$, TOC and $\%\text{CaCO}_3$) from the Shuqualak-Evans core (Mississippi, USA). Linnert et al. (2014) published a record of SSTs from this site, which they argued was largely controlled by global climate change. The comparison of this dataset with new data from the same core enables us to discuss the carbon-isotope record with regard to general global climate evolution. This discussion may help us to answer the question of whether prominent carbon-isotope excursions around the late Campanian–early Maastrichtian interval are related to the general trend of palaeotemperatures.

2. Geological setting and materials

During the Campanian–Maastrichtian, the Mississippi embayment was a relatively shallow epicontinental sea (Fig. 1) that covered much of the modern states of Louisiana, Mississippi and Florida. The Shuqualak-Evans core was drilled in Shuqualak, Mississippi, USA (32° 58' 49" N, 88° 34' 8" W), recovering a near-continuous, ~240 m-thick sequence of mainly Campanian and Maastrichtian marine sediments (Fig. 2). The base of the sequence (~253.2–252 m drilling depth) is characterised by glauconitic sandstones of latest Santonian–earliest Campanian age (Linnert et al. 2014). These sandstones are overlain by the lower Campanian Mooreville Formation (~252–180 m), which is mainly composed of marls and marly chalk. The lower Campanian Arcola Limestone was recovered between 180 m and 175 m. The interval from ~175 m to ~9 m belongs to the lower Campanian–upper Maastrichtian Demopolis Formation and is dominated by marls and chalks (Fig. 2). Calcareous nannofossil and planktonic foraminiferal biostratigraphy (Linnert et al. 2014), suggests that most of the cored interval (253.19 m–22.86 m) was deposited during the Campanian (83.2–72 Ma), whereas the entire Maastrichtian (72–66 Ma) is only represented by 13.41 m of sediment. For geochemical analyses, 160 samples were analysed from the core, at approximately 1.5 m resolution.

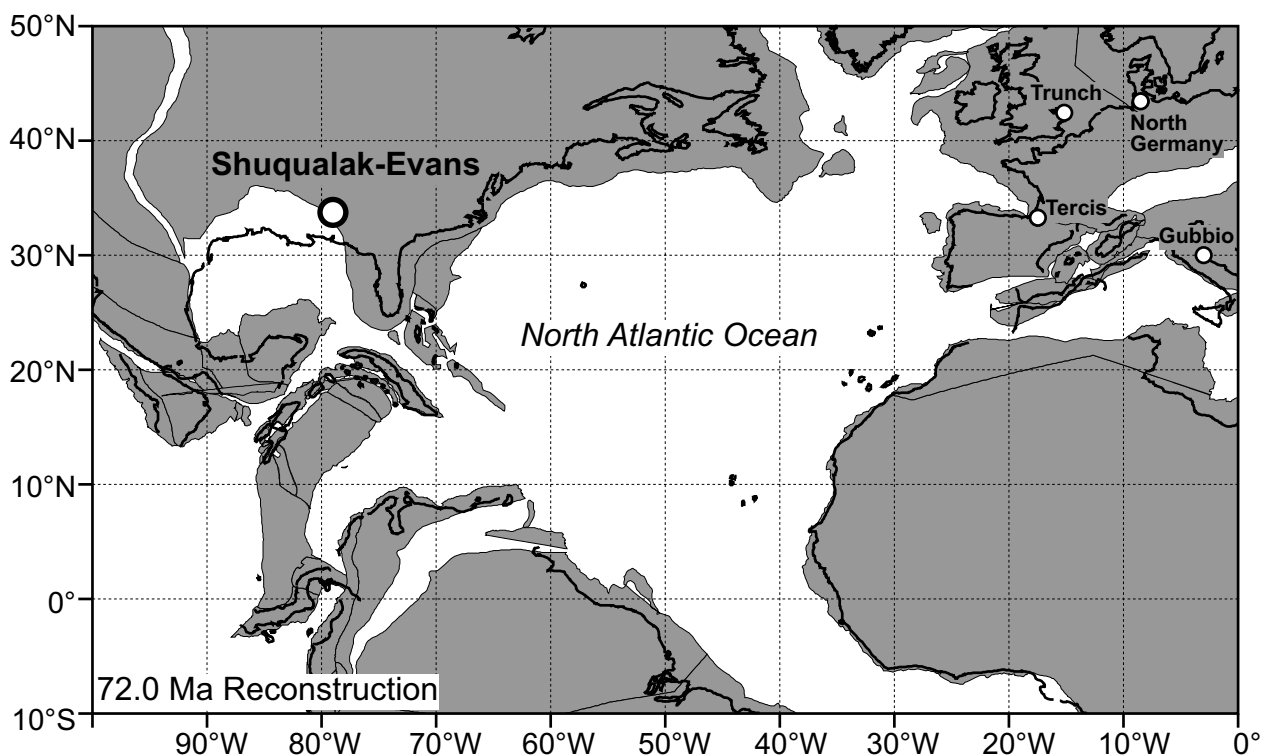


Fig. 1. Palaeogeographic map of the North Atlantic at 72.0 Ma (continental plates blocked out in grey, thick black lines indicate Present Day coastlines) indicating the locality of Shuqualak and other sections (North Sea, Tethys) discussed in the text. Reconstruction adapted from the Ocean Drilling Stratigraphic Network (ODSN) palaeomap project (<http://www.odsn.de/odsn/services/paleomap/paleomap.html>)

In addition to the data from the Shuqualak-Evans core, we also provide new stable-isotope data from between ~100 m and 150 m depth in the British Geological Survey Trunch core drilled through the English Chalk to increase the stratigraphic resolution through the Late Campanian carbon-isotope Event (LCE). The Trunch borehole is situated in Norfolk, UK and is one of the key records for Upper Cretaceous integrated stratigraphy (Jenkyns et al. 1994, Jarvis et al. 2002, 2006, Voigt et al. 2010, 2012).

3. Methods

3.1 Carbonate content and TOC

Total carbon (TC) and total organic carbon (TOC) were measured on each sample from the Shuqualak-Evans core to aid interpretation of the geochemical data. Bulk powdered samples were obtained by drilling fresh rock surfaces with a 0.5–1 mm drill-bit. Samples were analysed using a Thermo Flash EA 1112 elemental analyser in the laboratories at University

College London (UCL). For the TOC analysis, each sample was decarbonated in a silver foil capsule, using ~10% hydrochloric acid, and dried down on a hot-plate. TC was measured on unacidified samples in aluminium foil capsules. Total inorganic carbon (TIC) was calculated by the subtraction of TOC from the TC. Then by assuming that TIC to be associated with CaCO_3 , it was possible to calculate % CaCO_3 by simply multiplying TIC by 8.3333 (recurring; the carbon represents 1/8.333 part of the CaCO_3). Repeated analysis of internal standards suggest that the standard deviation on TC and TOC measurements is $\pm 0.1\%$.

3.2 Bulk carbonate stable isotopes ($\delta^{13}\text{C}$, $\delta^{18}\text{O}$)

One hundred and fifty-seven bulk-carbonate samples from the Shuqualak-Evans core were analysed by continuous-flow mass spectrometry, using a Gasbench connected to a Thermo Finnegan Delta+ XP mass spectrometer in the Bloomsbury Environmental Isotope Facility (BEIF) at UCL. Three hundred and sixty-two samples from the Trunch core were collected,

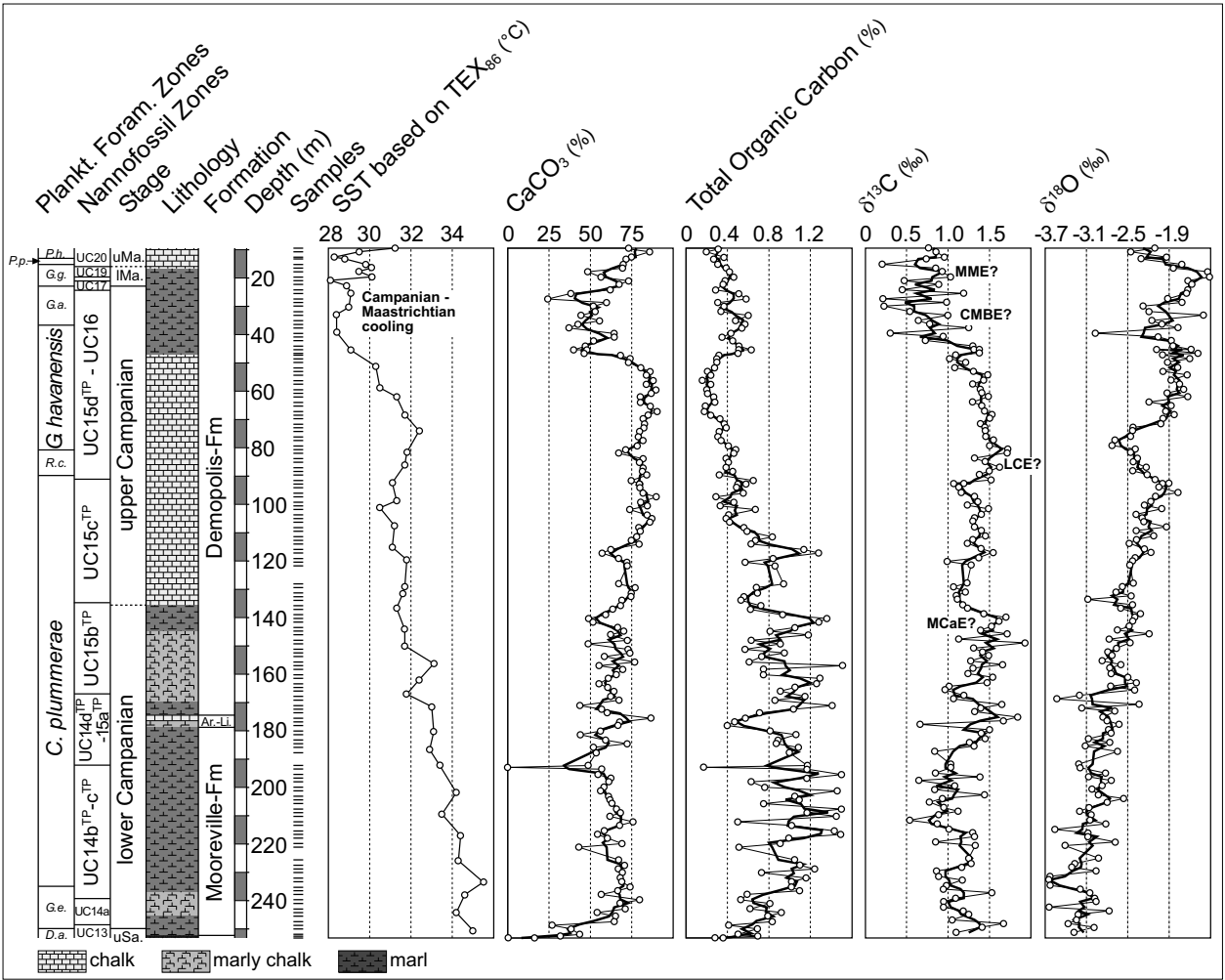


Fig. 2. Biostratigraphy, lithology and geochemistry of the Shuqualak-Evans core. Biostratigraphy and palaeo-SST estimates (based on TEX_{86}) after Linnert et al. (2014). Substages: uSa. – upper Santonian; lMa. – lower Maastrichtian; uMa. – upper Maastrichtian. Carbon-isotope events: MCaE – Mid-Campanian Event; LCE – Late Campanian Event; CMBE – Campanian Maastrichtian Boundary Event; MME – Mid-Maastrichtian Event. Planktonic foraminiferal zones: *D.a.* – *Dicarinella asymetrica*; *G.e.* – *Globotruncanella elevata*; *C.plummerae* – *Contusotruncana plummerae*; *R.c.* – *Radotruncana calcarata*; *G.havanensis* – *Globotruncanella havanensis*; *G.a.* – *Globotruncana aegyptiaca*; *G.g.* – *Gansserina gansseri*; *P.p.* – *Pseudoguembelina palpebra*; *P.h.* – *Pseudoguembelina hariaensis*.

where possible, every 10 cm between 99.2 and 152.3 m depth. These samples were analysed using a VG Isogas Prism II mass spectrometer with an on-line VG Isocarb common acid-bath preparation system at the Department of Earth Sciences, University of Oxford. All isotope data are reported in the standard delta notation ($\delta^{13}C$, $\delta^{18}O$) in per-mil (‰) values on the Vienna PDB (V-PDB) scale. One standard deviation error on internal standards at UCL was generally better than $\pm 0.05\text{‰}$ for $\delta^{13}C$ and $\pm 0.10\text{‰}$ for $\delta^{18}O$ and, at Oxford, was better than $\pm 0.1\text{‰}$ for both $\delta^{13}C$ and $\delta^{18}O$.

4. Results

4.1 TOC and $CaCO_3$ values

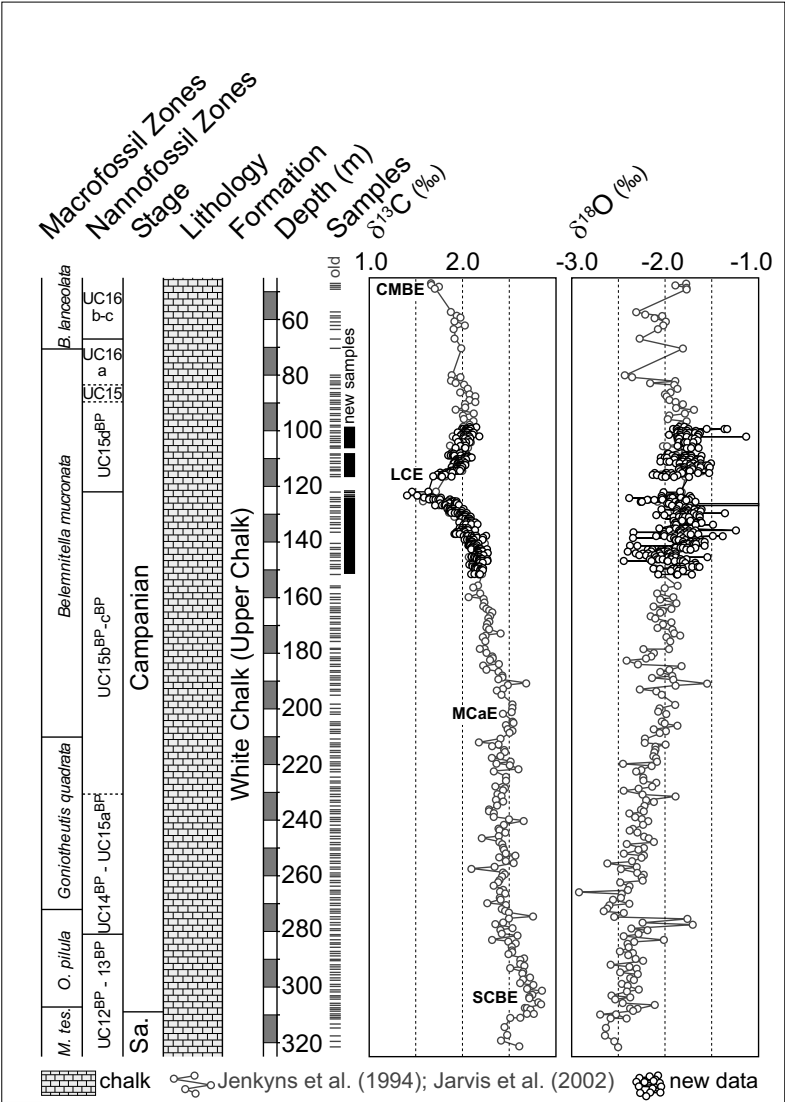
The stratigraphic variations in TOC and $\%CaCO_3$ from the Shuqualak-Evans core are shown in Figure 2 and provided in Supplementary Table 1. The glauconitic sandstone at the base of the core (253.19–252.83 m) is characterised by increasing carbonate content from 0.4% at 253.19 m to 16.2% at 252.83 m. The TOC of the sandstone varies from 0.3–0.4%. In the mostly marly Mooreville Formation (251.97–179.83 m), the

carbonate content varies from 0.0% (at 192.94 m) to 79.8% (at 239.27 m); the TOC values vary from 0.2% (at 192.94 m) to 1.5% (at 207.26 m and 195.07 m). The chalky Arcola Limestone (178.31–175.26 m) is characterised by high carbonate content, from 66.6% (at 178.31 m) to 86.8% (at 175.26 m) and lower TOC content of 0.4% (at 178.31 m) to 0.6% (at 175.26 m). In the Demopolis Formation (173.74–9.45 m), the carbonate content is more variable, with values from 24.2% (at 27.43 m) to 90.3% (at 67.06 m). In the Demopolis Formation, the chalky interval from 114.30 m to 47.24 m is characterised by values higher than 67.1%. In the marly interval from 46.94–18.29 m, the CaCO₃ content varies from 24.2% to 73.2%. The TOC shows a similar variability, with values from 0.2% (at 56.39 m) to 1.5% (at 156.97 m).

4.2 Stable isotopes ($\delta^{13}\text{C}$, $\delta^{18}\text{O}$) from the Shuqualak-Evans core

The stable-isotope records ($\delta^{13}\text{C}$, $\delta^{18}\text{O}$) from the Shuqualak-Evans core are generally independent of changes in lithology (Figure 2; data in Supplementary Table 1). The lowest value of $\delta^{13}\text{C}$ (−1.42‰) was measured in the lowermost analysed sample, at 252.83 m; this value rises to 1.10‰ in the next sample, at 251.46 m. The interval from 251.46–211.84 m is characterised by variable carbon-isotope values, but there is also a distinct decreasing trend from 1.67‰ at 248.41 m to 0.54‰ at 211.84 m. In the following sequence, from 211.84 m to 170.69 m, the $\delta^{13}\text{C}$ ratios are still highly variable, but they increase up to 1.84‰ at 175.26 m. The next interval, from 169.16 m to

Fig. 3. Biostratigraphy, lithology and geochemistry of the Trunch core, Norfolk, UK. Biostratigraphy after Jenkyns et al. (1994), Jarvis et al. (2002) and Voigt et al. (2010, 2012). Macrofossil zones: *B. lanceolata* – *Belemnella lanceolata*; *O. pilula* – *Offaster pilula*; *M. tes.* – *Marsupites testudinarius*.



140.21 m, starts with relatively low values of around 1.00‰ (lowest 0.97‰ at 166.12 m), but these values increase again towards 1.70‰. From 138.66 m to 92.81 m, the $\delta^{13}\text{C}$ data are generally lower, but more stable than in the older sediments; the lowest values were measured in the intervals from 137.16 m to 120.20 m (down to 0.99‰) and from 96.01 m to 92.81 m (down to 1.07‰). The interval from 91.44 m to 53.34 m is characterised by less-variable, but higher, $\delta^{13}\text{C}$ ratios, ranging from 1.30‰ (at 64.01 m) to 1.72‰ (at 80.77 m). From 53.34 m, the carbon-isotope data show another trend of decreasing values, which continues towards the top of the Shuqualak-Evans core. In this interval, the values become highly variable again, ranging from 0.21‰ (at 15.24 m) to 1.38‰ (at 46.94–45.72 m).

The $\delta^{18}\text{O}$ record also starts with the lowermost value (−5.82‰) at 252.83 m, jumping to −3.28‰ in the next sample at 251.46 m. From this sample upwards, $\delta^{18}\text{O}$ shows a distinctive trend towards higher values, up to 96.01 m (−1.77‰). The $\delta^{18}\text{O}$ record then decreases down to −2.73‰ at 79.25 m and increases again towards −1.48‰ at 46.94 m. The $\delta^{18}\text{O}$ values are highly variable in the highest part of the sequence (46.94–9.45 m), with minimum to maximum values ranging from −2.97‰ (at 39.62 m) to −1.32‰ (at 19.81 m). Both isotopic signatures of the Shuqualak-Evans core are given in Figure 2.

4.3 Stable isotopes ($\delta^{13}\text{C}$, $\delta^{18}\text{O}$) from the Trunch core

The new stable-isotope data from the Trunch core (Supplementary Table 2) agrees well with previously published data (Figure 3; Jenkyns et al. 1994). The higher resolution carbon-isotope stratigraphy of the LCE suggests that the magnitude of this event may have been slightly larger (by about 0.2‰) than estimated from the low-resolution dataset, but otherwise the new data do not significantly alter the view of the LCE.

5. Discussion

5.1 Is a primary carbon-isotope signal preserved in the Shuqualak-Evans core?

Before interpreting bulk-carbonate carbon-isotope data from the Shuqualak-Evans core as a primary seawater signal, it is necessary to consider whether sec-

ondary effects, such as the reworking/variable input of calcareous sediments and diagenesis, may have influenced the $\delta^{13}\text{C}$ data. The lack of evidence for reworking of pre-Campanian calcareous nannofossils and planktonic foraminifera (Linnert et al. 2014) indicates no significant deposition of allochthonous carbonates. There is little evidence for carbonate diagenesis from calcareous nannofossils and planktonic foraminifera because assemblages are almost exclusively very well preserved throughout the studied section. Only in the uppermost part of the studied section (9.45–22.86 m) does nannofossil preservation decline, although even here it is still relatively good. A reduction in the quality of carbonate preservation in this uppermost part of the core may also be indicated by more variable carbon-isotope values, which are possibly related to some degree of recrystallisation. Such an increased variability of $\delta^{13}\text{C}$ data is observed for the interval below 148 m and for samples above 50 m, both intervals of relatively low CaCO_3 and high TOC content (Fig. 2). These lower carbonate values may indicate an increased dilution by non-carbonate components, or a change in carbonate productivity, possibly driven by factors such as changing terrestrial run-off or surface-water circulation patterns. The carbon-isotope values are generally consistent with those of other Upper Cretaceous pelagic marls and chalks, and hemipelagic deposits, all interpreted as representing primary seawater signals (e.g., Jenkyns et al. 1994, Jarvis et al. 2002, 2006, Li et al. 2006, Voigt et al. 2010, 2012, Wendler et al. 2011), albeit 0.5–1‰ lighter.

The $\delta^{18}\text{O}$ values are generally consistent with carbonate formed from seawater, and are not anomalously isotopically light, as would be expected if the carbonate had been affected by extensive meteoric, or extreme burial, diagenesis. However, one data-point (occurring in the glauconitic sandstone at the base of the core) has distinctly lower $\delta^{13}\text{C}$ and $\delta^{18}\text{O}$ values compared to the rest of the dataset. This single data point may derive from carbonate that is not entirely marine in origin (the lithology of this sample indicates shallower-water deposition), and so is not included in the discussion of carbon-isotope stratigraphy that follows. Excluding this one sample, there is no significant correlation between $\delta^{13}\text{C}$ and $\delta^{18}\text{O}$ (Figure 4a), which suggests that the carbon-isotope data have not been affected by diagenesis, and so can be interpreted as a primary recorder of sea-water $\delta^{13}\text{C}$ (as discussed in many previous publications, including Veizer 1983 and Sharp 2006). Furthermore, cross-plots between geochemical ($\delta^{13}\text{C}$, $\delta^{18}\text{O}$) and lithological data (CaCO_3 ,

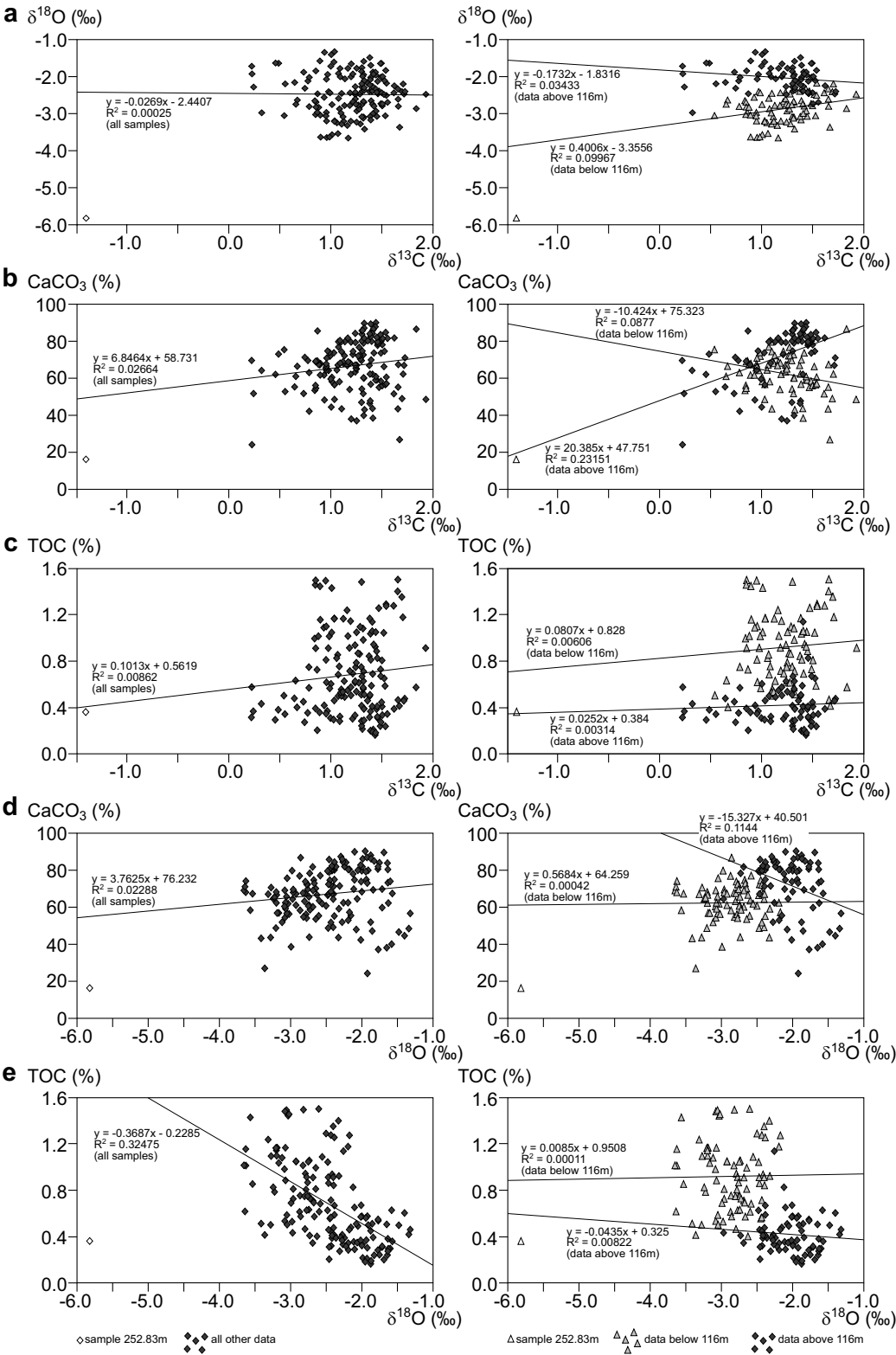


Fig. 4. Cross-plots of $\delta^{13}\text{C}$ (a) vs $\delta^{18}\text{O}$, (b) vs \%CaCO_3 , (c) vs TOC and $\delta^{18}\text{O}$, (d) vs \%CaCO_3 , (e) vs TOC. In the cross-plots on the left, linear regressions and R^2 -values were calculated for all measured samples, excluding sample 252.83 m; on the right, those regressions were calculated individually for all samples below 116 m (combined interval of highly variable carbon-isotope data below 148 m and low $\delta^{13}\text{C}$ values between 148 m and 116 m) and for all samples above 116 m (interval of interest containing the LCE and CMBE CIEs).

TOC) support the assertion that no strong diagenetic effect has influenced the isotopic values, as there is no significant correlation between any of these parameters (Figure 4b–e).

5.2 Carbon-isotope stratigraphy and refinement of the age-model for the Shuqualak-Evans core

Previous high-resolution studies of Upper Cretaceous carbon-isotope stratigraphy (e.g. Jarvis et al. 2002, 2006, Voigt et al. 2010, 2012, Thibault et al. 2012a, b, Wendler 2013) have revealed five to seven stratigraphically significant carbon-isotope excursions (CIEs) in the Santonian–Maastrichtian interval. These excursions include the Santonian–Campanian Boundary Event (SCBE, positive excursion), the LCE (negative excursion), the CMBE (negative excursion), the Mid-Maastrichtian Event (MME, a two step positive excursion) and the Cretaceous–Paleogene Boundary Event (KPgE, major negative excursion; e.g. Jarvis et al. 2002, Voigt et al. 2010, 2012). Further isotopic anomalies are described in the work of Jarvis et al. (2002) and Thibault et al. (2012a, b), including the Mid-Campanian Event (MCaE, positive excursion) and the latest Campanian Epsilon Event (CEE, negative excursion).

The uppermost ~40 m of the Shuqualak-Evans core are difficult to correlate with certainty, due to the relatively condensed nature of the Maastrichtian sequence (Linnert et al. 2014). Carbon-isotope values are generally relatively light, albeit with some scatter. Slightly higher $\delta^{13}\text{C}$ values between ~16 m and 20 m may correlate with the MME, as the base occurrence of *Lithra- phidites quadratus* (nannofossil) is at 16.76 m, which is associated with the MME elsewhere (Voigt et al. 2012).

The most striking feature of the carbon-isotope record is the shift towards more negative $\delta^{13}\text{C}$ values between 50 m and 40 m depth (Figs. 2, 4). Above this transition, at approximately 23 m depth, Linnert et al. (2014) reported top *Uniplanarius trifidus*, top *Tranolithus orionatus* (nannofossils) and base *Gansserina gansseri* (planktonic foraminifer) (Fig. 5). Voigt et al. (2012) discussed the relative merits of these biostratigraphic markers and suggested that all three are closely associated with the CMBE, indicating that the negative excursion between 50 m and 40 m can be correlated with the onset of this global CIE.

A second small negative excursion, which shows a similar magnitude to the LCE in European sections

(including the high resolution record from the Trunch borehole; Figures 3 and 5) is observed in the Shuqualak-Evans core at ~90–100 m depth. This isotope anomaly, however, occurs well below the bases of the two index taxa *Radotruncana calcarata* (planktonic foraminifer, 89.89 m) and *Uniplanarius trifidus* (calcareous nannofossil, 91.44 m; Linnert et al. 2014), which constrain the stratigraphic position of the LCE at other localities. According to data from those other localities, the LCE appears within (Gubbio, Italy and Shatsky Rise, NW Pacific), or above (Tercis, France and Tibet), the *R. calcarata* planktonic foraminiferal zone (Wendler et al. 2011, Voigt et al. 2012, Wendler 2013). Thus, it is unlikely that the $\delta^{13}\text{C}$ excursion below ~90 m represents the LCE, as defined by Voigt et al. (2012), unless a minor hiatus exists. However, based on the biostratigraphy, the LCE may be recorded in Shuqualak by a weak negative excursion (~82–88 m, Fig. 5) within the *R. calcarata* zone. If correct, then this would suggest a much less significant LCE, compared to the magnitude of the excursion in European sections.

An alternative definition for the LCE is given by Thibault et al. (2012a), who suggested a longer duration for the event, beginning with a small negative $\delta^{13}\text{C}$ excursion, followed by a short recovery interval and, in the European sections, by a much more pronounced second negative excursion. A similar LCE definition is also used by Chenot et al. (2016), who termed the older, smaller peak the “pre-LCE” and the younger, larger excursion the “LCE main”. The minor pre-LCE, which is closely associated with the base of *U. trifidus*, is well developed at Tercis and in northern Germany (see Fig. 4 in Thibault et al. 2012a; see Figs. 3, 6 in Voigt et al. 2012). At Shuqualak, the pre-LCE excursion (Fig. 5) is perhaps represented by the distinctive isotope anomaly measured below 90 m. In contrast to European sections, the LCE from Mississippi may begin with a well-pronounced pre-LCE, followed by a much weaker LCE main (Figs. 5, 6). However, there are still some discrepancies about this interpretation and the position of the *R. calcarata* Zone because, in some European sections, the pre-LCE appears well within that biozone (e.g., Tercis; Thibault et al. 2012a, Voigt et al. 2012, Chenot et al. 2016), whereas in Shuqualak it lies below that biozone.

Some diachroneity of the *R. calcarata* biozone is perhaps related to local palaeoenvironmental stress (i.e. relatively shallow water depths, eutrophic vs. oligotrophic conditions, water mass stratification ...) affecting the stratigraphic appearance of *R. calcarata*.

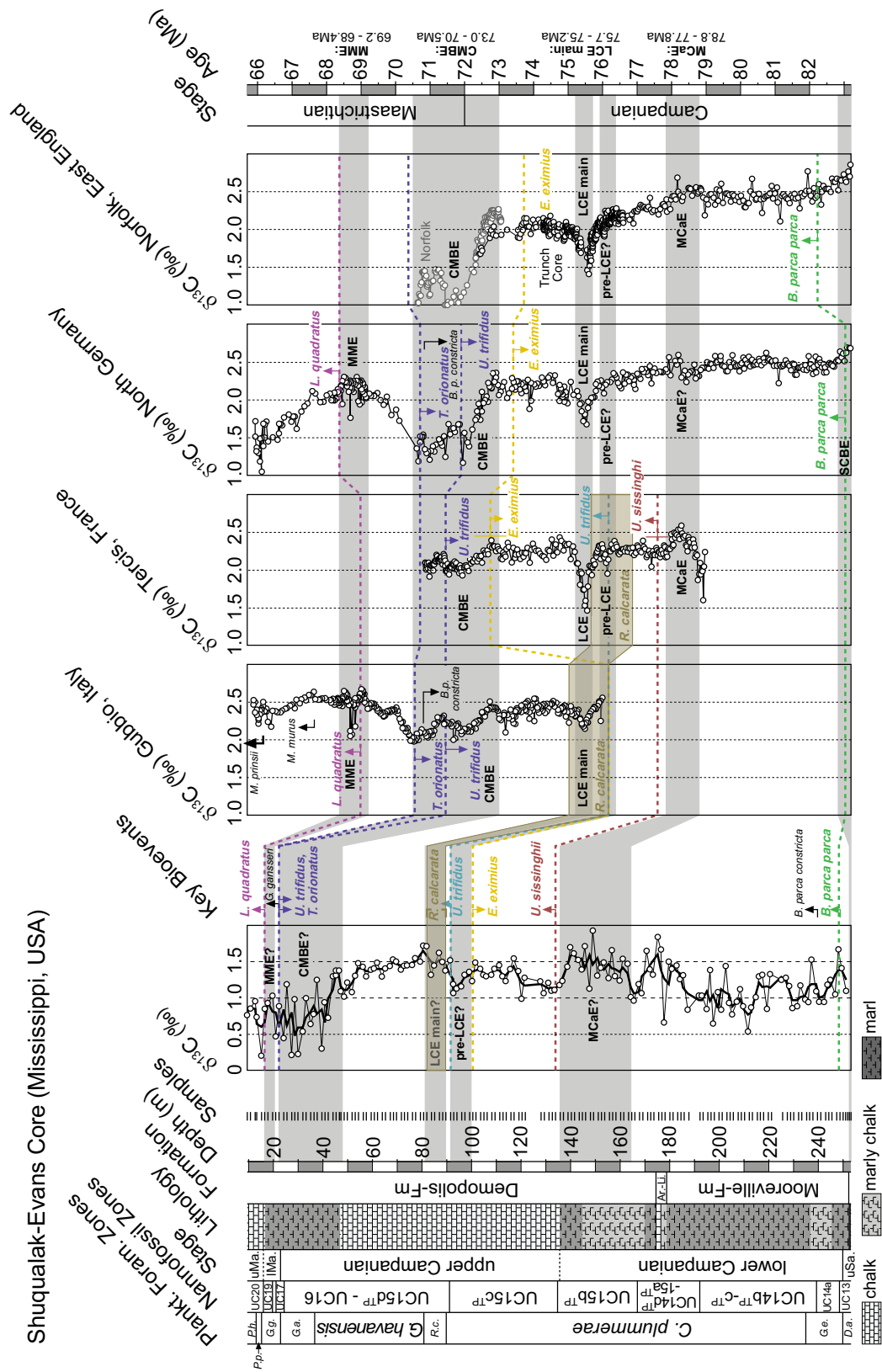


Fig. 5. Correlation of the carbon-isotope record from Shuqualak (this study) with various published European datasets (after Voigt et al., 2010, 2012). The Shuqualak $\delta^{13}\text{C}$ data are plotted as a three-point running mean (bold black line) and as individual data points (thin black line with open circles) against depth. Previous data (Gubbio, Italy; Tercis, France; northern Germany; eastern England: after Jarvis et al. 2002, Voigt et al. 2010, 2012) are plotted using the age-model of Voigt et al. (2012); samples older than 79 Ma are interpolated by using the GTS age of the Santonian–Campanian boundary (83.6 Ma: Gradstein et al. 2012). Carbon-isotope events – see text. Calcareous nanofossil datums: *B. p. constricta* – *Broinsonia parca constricta*; *E. eximius* – *Eiffellithus eximius*; *L. quadratus* – *Lithraphidites quadratus*; *M. murus* – *Micula murus*; *M. prinsii* – *Micula prinsii*; *R. levis* – *Reinhardtites levis*; *T. orionatus* – *Tranolithus orionatus*; *U. trifidus* – *Uniplanarius trifidus*. Planktonic foraminifera datums: *G. gansseri* – *Gansserina gansseri*; *R. calcarata* – *Radotruncana calcarata*. Green band marks the full range of *R. calcarata*.

This is supported by the observation that the genera *Globotruncana*, *Globotruncanita*, and *Globotruncanella*, which are usually common in late Campanian deeper-water settings (Abramovich et al. 2003, 2010, Pérez-Rodríguez et al. 2012), are only represented in Shuqualak Evans by a few specimens each, suggesting conditions were not suitable for all planktonic foraminifera. Thus, it is possible that the stratigraphic range of *R. calcarata* is shorter in Shuqualak than in other North Atlantic localities due to local conditions.

The higher $\delta^{13}\text{C}$ values below base *U. sissinghii* (at 134.11 m; Fig. 5) may correlate with the MCaE, which was observable in the same stratigraphic position at Tercis (see Fig. 3 in Voigt et al. 2012). At Tercis, the lower boundary of the MCaE is defined by a negative excursion (see Fig. 4 in Thibault et al. 2012a). Such a negative peak is observed in the Shuqualak-Evans core at ~165 m. The MCaE is not as well constrained as the younger events, however, having only been previously documented in France (Thibault et al. 2012a) and England (Jenkyns et al. 1994, Jarvis et al. 2002). The older SCBE, which was originally described from below base *Broinsonia parca* subsp. *parca* (nannofossil) (Jarvis et al. 2002, Voigt et al. 2010), was not encountered in the Shuqualak carbon-isotope record, as only a few samples were measured below that bioevent (248.41 m). The sedimentary record below 248.41 m is increasingly discontinuous as the basal sediments are highly condensed, glauconite rich and interrupted by several hiatuses. Whereas sample 249.94 m is dated as Campanian, sample 251.46 m is supposedly of latest Santonian age due to the presence of the Santonian planktonic foraminifer *Dicarinella asymetrica*. The coeval occurrence of early Campanian nannofossil species *Arkhangelskiella cymbifomis* in the same samples (251.46–253.19 m) suggests that the basal sediments from Shuqualak were deposited during the Santonian–Campanian transition.

Our isotope calibration of the Shuqualak-Evans core implies that the age-model published in Linnert et al. (2014) should be subtly refined, especially for the late Campanian–early Maastrichtian interval. In addition to calcareous nannofossil and planktonic foraminifer bioevents, the new model also considers the onset of the CMBE as a tie point, which was, following Voigt et al. (2012), set to 73 Ma. Our revised age-model (Fig. 6 and Supplementary Table 3) suggests that sedimentation rates were highest in the early Campanian (~2.8 cm/kyr for the interval 251.5–84 m), decreased during the late Campanian (~1.3 cm/kyr for the interval 84–29 m and ~0.5 cm/kyr for the inter-

val 29–17 m) and were lowest in the Maastrichtian (~0.2 cm/kyr).

5.3 The local depositional environment and its influence on the $\delta^{13}\text{C}$ record

Voigt et al. (2012) discussed how the magnitude of the latest Cretaceous CIEs vary regionally, perhaps due to local environmental overprints on the global CIEs. For example, the largest magnitude of the CMBE, greater than 1‰, was measured in shallow-shelf sections from the North Sea area (Trunch and the Norfolk coast; northern Germany; Stevns-1, Denmark) and in deep-waters of the Southern Ocean. Lower magnitudes were observed in Tethyan and Pacific sections (Gubbio, Tercis, and Ocean Drilling Program Site 1210 on Shatsky Rise in the NW Pacific; Voigt et al. 2012). The magnitude of the CMBE (~–1.0‰) in the Shuqualak-Evans record is similar to that observed in the North Sea area (Voigt et al. 2012) and is consistent with similar shelf palaeoenvironments. This relatively high value provides further support for the idea postulated by Voigt et al. (2012), that shallow-marine carbon reservoirs were more sensitive to local processes, such as the local oxidation of organic matter, than open-ocean sites. Furthermore, local palaeoceanographic conditions in the Mississippi embayment (e.g., productivity, remineralisation in the water column, surface-water mass circulation patterns from areas with low surface $\delta^{13}\text{C}$) may, in conjunction with differential diagenesis, explain why the Shuqualak-Evans core exhibits $\delta^{13}\text{C}$ values that are typically 0.5 to 1‰ less than coeval strata elsewhere.

5.4 Testing theories about palaeoenvironmental triggers of the CMBE and LCE

Even though the CMBE is well known from various localities around the world (Jarvis et al. 2002, Voigt et al. 2010, 2012, Thibault et al. 2012a, b, Jung et al. 2013), there is still ongoing controversy concerning the causal mechanisms. At Shuqualak, the direct comparison of carbon isotope data with palaeo-SST estimates (TEX₈₆; Linnert et al. 2014) reveals that the CMBE is linked to the latest Campanian cooling. The isotope perturbation was associated with an interval of minimum SSTs, but commenced roughly 1–2 Myrs after the onset of the cooling event (Fig. 6). This observation from Shuqualak confirms previous results from the tropical Pacific (e.g. Jung et al. 2013), which also suggested a lag of approximately 1 Myr between the

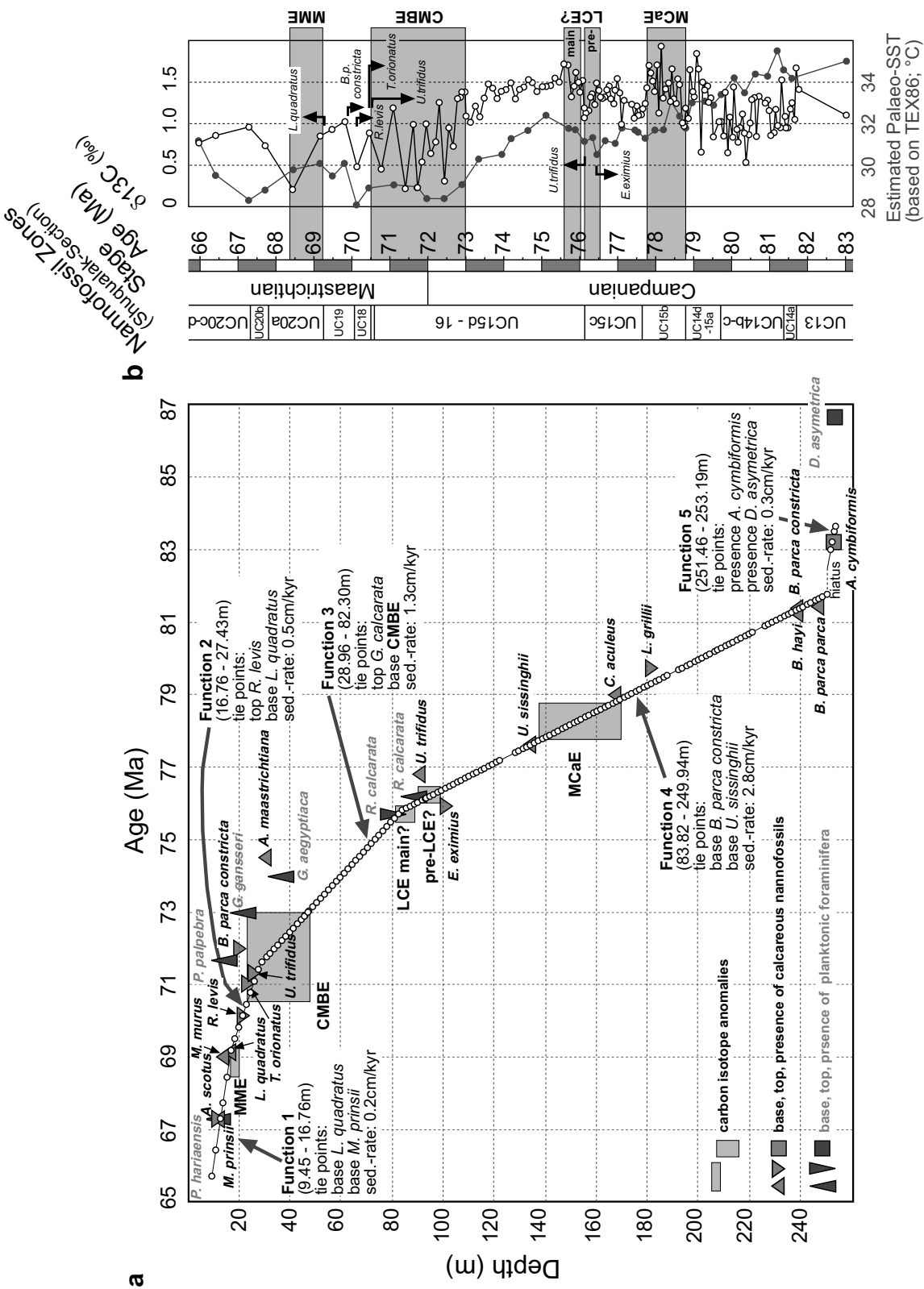


Fig. 6. Revised age-model for the Shuqualak-Evans core. (a) Age–depth plot for the Shuqualak-Evans section, with solid lines representing the age model, dots being the individual samples. Bioevents are given as bases and tops, age-calibrated using GTS2012 (Gradstein et al. 2012). CIEs are shown as grey blocks defined at depths in which they are interpreted in the Shuqualak-Evans core and the ages are as given in Voigt et al. (2012). (b) Carbon-isotope results and TEX₈₆ palaeotemperature data (after Linnert et al. 2014) plotted against age (Ma) from our revised age-model. The intervals of the CIEs after Voigt et al. (2012) are highlighted in grey.

onset of temperature change and the isotope excursion. This indicates that the temporal offsets between temperature change and carbon cycling during the CMBE were not restricted to the Pacific Ocean but were likely a global phenomenon. Such a relationship provides an important constraint on the processes triggering the CMBE.

Jarvis et al. (2002, 2006) suggested that the CMBE was mainly the consequence of eustatic sea-level falls, promoting lowland erosion and the oxidation of organic matter. It has been suggested that the eustatic sea-level falls were caused by the thermal contraction of the water-column, due to global cooling or by glacio-eustasy (e.g., Barrera et al. 1997, Miller et al. 1999, 2005, Browning et al. 2008). However, a glacial-eustatic mechanism seems unlikely given the lag between the onset of cooling and the CMBE. A lag of approximately 1 Myr is too long to be consistent with the build up of continental ice-sheets and sea-level fall, as this would likely have occurred over some tens of thousands of years. Similarly, the temporal lag also precludes sea-level falls due to thermal contraction of the water-column, given that the cooling and lag are observed in both SST and bottom-water records. Further arguments against a glacio-eustatic model are given by relatively warm deep-water temperatures (6–10°C; Huber et al. 1995, 2002, Miller et al. 2005, Friedrich et al. 2012), warm Arctic Ocean SSTs (Jenkyns et al. 2004), cool-temperate mean annual air temperatures on the Antarctic Peninsula (> 7°C; Francis and Poole 2002, Kemp et al. 2014) and the relatively long duration (> 2 myr) of the CMBE (Voigt et al. 2012). Although other mechanisms of driving sea-level change in the Cretaceous have been proposed (recently discussed by Wagreich et al. 2014, Sames et al. 2016, Wendler and Wendler 2016), such as “limno-eustasy” or “aquifer-eustasy”, these mechanisms also seem unlikely, given the duration of the CMBE and the lag between climatic and carbon-cycle events.

Alternatively, it has been suggested that CIEs in the Campanian–Maastrichtian (e.g., CMBE) were the result of large-scale, solid-earth processes related to changes in plate tectonic configuration, subduction or hot-spot volcanism (Frank and Arthur 1999, Voigt et al. 2012, Jung et al. 2013). The long lag time between cooling and the onset of the CMBE may support such an explanation, as both climate change and carbon-cycle perturbation may have been coupled to certain stages of the same long-term tectonic change. For example, via the alteration of ocean circulation and ocean chemistry, solid earth processes could have in-

fluenced the production, preservation and burial of organic and carbonate carbon in shelf and deep-sea settings, and consequently the isotopic composition of the ocean-atmosphere reservoir (discussed in Jarvis et al. 2002). The exact nature of these changes in carbon cycling were likely rather complex, due to the interactions between relatively long-term changes in boundary conditions (e.g., changes in spreading rate and opening of gateways; Larson 1991, Frey et al. 2000, Coffin et al. 2002, Müller et al. 2008) and shorter term processes (e.g. reconfiguration of ocean circulation, changes in bottom-water chemistry: Barrera and Savin 1999, Friedrich et al. 2009, Robinson et al. 2010, Robinson and Vance 2012, Murphy and Thomas 2012, 2013, Jung et al. 2013).

What *is* clear is that the currently available data for the Campanian–Maastrichtian events cannot be reconciled with a simplistic interpretation of the carbon-isotope data alone. Commonly invoked mechanisms for negative CIEs, such as, oxidation of organic carbon, release of methane hydrates, and increased volcanism, would all lead to an increase in CO₂ in the ocean-atmosphere carbon reservoir that would be expected to cause synchronous warming during the negative $\delta^{13}\text{C}$ event. However, warming is not observed; on the contrary, there is evidence from Mississippi (Linnert et al. 2014), the Pacific Ocean (Jung et al. 2013), northern Germany (Voigt et al. 2010) and the Indian Ocean (Clarke and Jenkyns 1999, Falzoni et al. 2016) that the CMBE is linked to an interval of relatively cool temperatures. The significant duration of this negative CIE during the Campanian–Maastrichtian, compared, for example, to Palaeogene hyperthermals, allows other mechanisms of perturbing the carbon cycle to be explored. A mechanism must be invoked that does not cause a rise in atmospheric CO₂, but does cause a small negative $\delta^{13}\text{C}$ excursion in DIC globally and, for the CMBE at least, a drop in atmospheric CO₂ (see Hasegawa et al. 2003).

At present, it is difficult to ascribe a precise solution, but it is interesting to note that a number of studies have suggested that the CMBE was associated with an increased influence of southerly-sourced deep-waters (e.g. Barrera and Savin 1999, Frank and Arthur 1999, Jung et al. 2013). Most of these models suggest that the latest Cretaceous cooling raised the latitudinal thermal gradient, which led to an increase in the influence of global deep-water masses formed in southern high-latitude sources (Huber et al. 1995, 2002, Linnert et al. 2014). The presence of well-oxygenated southerly deep-waters could have resulted in a better ventilat-

ed and less corrosive deep-ocean. If so, average rates of global organic-carbon respiration and carbonate burial would have increased, assuming that they were not offset by a slowing of deep-ocean circulation elsewhere. These rate changes would have had the effect of reducing organic-carbon burial rates, relative to carbonate burial, and thus reducing $\delta^{13}\text{C}$ values (Jarvis et al. 2002). A simple isotopic mass balance (e.g., the approach of Kump and Arthur 1999) shows that decreasing organic-carbon burial rates necessitates an increase in carbonate burial with an isotopically lighter value, assuming all other fluxes and reservoirs remain constant. Additional carbon-cycle and earth-system modelling is required to ascertain whether this mechanism can account for the CMBE and the absence of warming during that negative CIE over appropriate timescales.

The LCE is more difficult to explain, as it shows different patterns in Europe and North America (see discussion above). Our data from Shuqualak indicate that, around the LCE, there is a cooling event, but the difficulties of correlating Shuqualak with other records precludes a more definitive assessment. If our correlation is correct, then the relationship between the LCE and climate may be similar to that invoked for the CMBE, with a similar lag between climate change and carbon cycling (Fig. 6). An alternative model for the LCE (both pre-LCE and LCE main) proposed by Chenot et al. (2016) invokes a relationship between these CIEs and an interval of enhanced weathering in Europe and parts of the Tethyan Realm. This enhancement of weathering was perhaps the consequence of tectonic activity, a sea-level lowstand (Chenot et al. 2016) or a more humid climate. Two of these possible factors (tectonics, local climate) are region-dependent; thus they may have had different patterns in Europe and in North America. Differences in those factors may have therefore been responsible for the different shapes of the LCE in different oceanographic regions. Further local palaeoenvironmental parameters, that may have also caused different patterns in the carbon-isotope record, include water depth, productivity, remineralisation in the water column, surface-water mass circulation patterns from areas with low surface $\delta^{13}\text{C}$, and 'seawater ageing' (e.g., Holmden et al. 1998, Voigt et al. 2012).

6. Conclusion

The Campanian–Maastrichtian carbon-isotope record from the Shuqualak–Evans core contains local expressions of the MCaE, the LCE, the CMBE and the MME, thereby adding to evidence from the Atlantic, Pacific and Tethyan Oceans for the global significance of these CIEs. The comparison of carbon-isotope and TEX_{86} data demonstrates that two of these events (LCE, CMBE) occurred during intervals of cooler temperatures, suggesting a possible role for climate change in their genesis. However, significant temporal offsets between the cooling of both bottom and surface waters and the negative CIEs suggest that a simple cause-and-effect relationship, such as might be imagined through glacio-eustasy, is unlikely. Rather, in keeping with some previous studies, we suggest that both these CIEs were the result of a more protracted sequence of events linking tectonic (sea-floor spreading, oceanic gateways), palaeoclimatic (Campanian–Maastrichtian cooling) and palaeoceanographic processes. An altered global oceanic circulation may have then affected bottom-water chemistry, leading to changes in the global ratio of carbonate to organic-carbon burial that ultimately drove the negative CIEs. However, unlike some negative CIEs in Earth history (e.g. the Paleocene–Eocene Thermal Maximum), there is no sign of global warming and no evidence for excess carbon input into the atmosphere during the CMBE and LCE intervals. The Late Cretaceous events described here clearly demonstrate that not all negative carbon-isotope excursions conform to the same model and that a better understanding of all these events is required to improve the interpretations of small negative CIEs throughout Earth history.

Acknowledgements. We thank Kevin Stevens for his thoughtful discussions and suggestions about the subject of isotope geochemistry. The support in the BEIF at UCL of Tony Osborn, Dorinda Ostermann and Tim Atkinson is gratefully acknowledged. Financial support is acknowledged from the German Science Foundation (DFG Research Stipend Li 2177/1-1 to CL), a Royal Society (UK) URF (to SAR), a NERC (UK) grant (to JAL and PRB), The Curry Fund of UCL (to CL), and MINECO/FEDER, UE (under project CGL2015-64422-P to JAA, SAR). We are very grateful to David Dockery from the Office of Geology, Mississippi Department of Environmental Quality for facilitating access to the Shuqualak–Evans core, to the late Ernie Russell for alerting us to the existence of this material, and to the British Geological Survey for allowing sampling of the Trunch core.

References

- Abramovich, S., Keller, G., Stüben, D., Berner, Z., 2003. Characterization of late Campanian and Maastrichtian planktonic foraminiferal depth habitats and vital activities based on stable isotopes. *Palaeogeography, Palaeoclimatology, Palaeoecology* 202, 1–29.
- Abramovich, S., Yovel-Corem, S., Almogi-Labin, A., Benjamini, C., 2010. Global climate change and planktic foraminiferal response in the Maastrichtian. *Paleoceanography* 25, PA2201.
- Ando, A., Woodard, S.C., Evans, H.F., Littler, K., Herrmann, S., MacLeod, K.G., Kim, S., Khim, B.-K., Robinson, S.A., Huber, B.T., 2013. An emerging palaeoceanographic ‘missing link’: Multidisciplinary study of rarely recovered parts of a deep-sea Santonian–Campanian transition from Shatsky Rise. *Journal of the Geological Society* 170, 381–384.
- Barrera, E., Savin, S.M., 1999. Evolution of late Campanian–Maastrichtian marine climates and oceans. In: Barrera, E., Johnson, C.C. (Eds.), *Evolution of the Cretaceous ocean-climate system*. Geological Society of America Special Paper 332, 245–282.
- Barrera, E., Savin, S.M., Thomas, E., Jones, C.E., 1997. Evidence for thermohaline-circulation reversals controlled by sea-level change in the latest Cretaceous. *Geology* 25, 715–718.
- Barron, E.J., 1983. A warm, equable Cretaceous: the nature of the problem. *Earth-Science Reviews* 19, 305–338.
- Barron, E.J., Thompson, S.L., Schneider, S.H., 1981. An ice-free Cretaceous? Results from climate model simulations. *Science* 212, 501–508.
- Berner, R.A., Kothavala, Z., 2001. Geocarb III: A revised model of atmospheric CO₂ over Phanerozoic time. *American Journal of Science* 301, 182–204.
- Bice, K.L., Huber, B.T., Norris, R.D., 2003. Extreme polar warmth during the Cretaceous greenhouse? Paradox of the late Turonian $\delta^{18}\text{O}$ record at Deep Sea Drilling Project Site 511. *Paleoceanography* 18, 1031, doi:10.1029/2002PA000848, 2003.
- Bornemann, A., Norris, R.D., Friedrich, O., Beckmann, B., Schouten, S., Damsté, J.S.S., Vogel, J., Hofmann, P., Wagner, T., 2008. Isotopic Evidence for Glaciation During the Cretaceous Supergreenhouse. *Science* 319, 189–192.
- Browning, J.V., Miller, K.G., Sugarman, P.J., Kominz, M.A., McLaughlin, P.P., Kulpecz, A.A., Feigenson, M.D., 2008. 100 Myr record of sequences, sedimentary facies and sea level change from Ocean Drilling Program onshore coreholes, US Mid-Atlantic coastal plain. *Basin Research* 20, 227–248.
- Chenot, E., Pellenard, P., Martinez, M., Deconinck, J.-F., Amiotte-Suchet, P., Thibault, N., Bruneau, L., Cocquerez, T., Laffont, R., Pucéat, E., Robaszynski, F., 2016. Clay mineral and geochemical expressions of the “Late Campanian Event” in the Aquitaine and Paris basins (France): Palaeoenvironmental implications. *Palaeogeography, Palaeoclimatology, Palaeoecology* 447, 42–52.
- Clarke, L.J., Jenkyns, H.C., 1999. New oxygen isotope evidence for long-term Cretaceous climatic change in the Southern Hemisphere. *Geology* 27, 699–702.
- Coffin, M.F., Pringle, M.S., Duncan, R.A., Gladchenko, T.P., Storey, M., Müller, R.D., Gahagan, L.A., 2002. Kerguelen Hotspot magma output since 130 Ma. *Journal of Petrology* 43, 1121–1139.
- Coffin, M.F., Duncan, R.A., Eldholm, O., Fitton, J.G., Frey, F.A., Larsen, H.C., Mahoney, J.J., Saunders, A.D., Schlich, R., Wallace, P.J., 2006. Large igneous provinces and scientific ocean drilling, status quo and a look ahead. *Oceanography* 19, 150–160.
- Cramer, B.S., Toggweiler, J.R., Wright, J.D., Katz, M.E., Miller, K.G., 2009. Ocean overturning since the Late Cretaceous: Inferences from a new benthic foraminiferal isotope compilation. *Paleoceanography*, 24, PA4216, doi:10.1029/2008PA001683.
- Donnadieu, Y., Pucéat, E., Moiroud, M., Guillocheau, F., Deconinck, J.-F., 2016. A better-ventilated ocean triggered by Late Cretaceous changes in continental configuration. *Nature Communications* 7, 10316, doi:10.1038/ncomms10316.
- Falzone, F., Petrizzo, M.R., Clarke, L.J., MacLeod, K.G., Jenkyns, H.C., 2016. Long-term Late Cretaceous oxygen- and carbon-isotope trends and planktonic foraminiferal turnover: A new record from the southern midlatitudes. *GSA Bulletin* 128, 1725–1735.
- Forster, A., Schouten, S., Baas, M., Sinninghe Damsté, J.S., 2007. Mid-Cretaceous (Albian–Santonian) sea surface temperature record of the tropical Atlantic Ocean. *Geology* 35, 919–922.
- Francis, J.E., Poole, I., 2002. Cretaceous and early Tertiary climates of Antarctica: evidence from fossil wood. *Palaeogeography, Palaeoclimatology, Palaeoecology* 182, 47–64.
- Frank, T.D., Arthur, M.A., 1999. Tectonic forcings of Maastrichtian ocean-climate evolution. *Paleoceanography* 14, 103–117.
- Frey, F.A., Coffin, M.F., Wallace, P.J., Weis, D., Zhao, X., Wise Jr., S.W., Wähnert, V., Teagle, D.A.H., Saccocia, P.J., Reusch, D.N., Pringle, M.S., Nicolaysen, K.E., Neal, C.R., Müller, R.D., Moore, C.L., Mahoney, J.J., Keszthelyi, L., Inokuchi, H., Duncan, R.A., Delius, H., Damuth, J.E., Damasceno, D., Coxall, H.K., Borre, N.K., Boehm, F., Barling, J., Arndt, N.T., Arntretter, M., 2000. Origin and evolution of a submarine large igneous province: the Kerguelen Plateau and Broken Ridge, southern Indian Ocean. *Earth and Planetary Science Letters* 176, 73–89.
- Friedrich, O., Herrle, J.O., Wilson, P.A., Cooper, M.J., Erbacher, J., Hemleben, C., 2009. The early Maastrichtian carbon cycle perturbation and cooling event: Implications from the South Atlantic Ocean. *Paleoceanography* 24, PA2211, doi:10.1029/2008PA001654.
- Friedrich, O., Norris, R.D., Erbacher, J., 2012. Evolution of middle to Late Cretaceous oceans – A 55 m.y. record of Earth’s temperature and carbon cycle. *Geology* 40, 107–110.

- Gradstein, F.M., Ogg, J.G., Schmitz, M., Ogg, G., 2012. The Geological Time Scale 2012. Elsevier Science Ltd., Boston, 1144 pp.
- Hasegawa, T., Pratt, L.M., Maeda, H., Shigeta, Y., Okamoto, T., Kased, T., Uemura, K., 2003. Upper Cretaceous stable carbon isotope stratigraphy of terrestrial organic matter from Sakhalin, Russian Far East: a proxy for the isotopic composition of paleoatmospheric CO₂. *Palaeogeography, Palaeoclimatology, Palaeoecology* 189, 97–115.
- Hay, W.W., 2008. Evolving ideas about the Cretaceous climate and ocean circulation. *Cretaceous Research* 29, 725–753.
- Hay, W.W., 2011. Can humans force a return to a ‘Cretaceous’ climate? *Sedimentary Geology* 235, 5–26.
- Hay, W.W., Floegel, S., 2012. New thoughts about the Cretaceous climate and oceans. *Earth-Science Reviews* 115, 262–272.
- Holmden, C., Creaser, R.A., Muehlenbachs, K., Leslie, S.A., Bergström, S.M., 1998. Isotopic evidence for geochemical decoupling between ancient epeiric seas and bordering oceans: Implications for secular curves. *Geology* 26, 567–570.
- Huber, B.T., Hodell, D.A., Hamilton, C.P., 1995. Middle–Late Cretaceous climate of the southern high latitudes: Stable isotopic evidence for minimal equator-to-pole thermal gradients. *Geological Society of America Bulletin* 107, 1164–1191.
- Huber, B.T., Norris, R.D., MacLeod, K.G., 2002. Deep-sea paleotemperature record of extreme warmth during the Cretaceous. *Geology* 30, 123–126.
- Jarvis, I., Mabrouk, A., Moody, R.T.J., de Cabrera, S., 2002. Late Cretaceous (Campanian) carbon isotope events, sea-level change and correlation of the Tethys and Boreal realms. *Palaeogeography, Palaeoclimatology, Palaeoecology* 188, 215–248.
- Jarvis, I., Gale, A.S., Jenkyns, H.C., Pearce, M.A., 2006. Secular variation in Late Cretaceous carbon isotopes: a new $\delta^{13}\text{C}$ carbonate reference curve for the Cenomanian–Campanian (99.6–70.6 Ma). *Geological Magazine* 143, 561–608.
- Jenkyns, H.C., Gale, A.S., Corfield, R.M., 1994. Carbon- and oxygen-isotope stratigraphy of the English Chalk and Italian Scaglia and its palaeoclimatic significance. *Geological Magazine* 131, 1–34.
- Jenkyns, H.C., Forster, A., Schouten, S., Sinninghe Damsté, J.S., 2004. High temperatures in the Late Cretaceous Arctic Ocean. *Nature* 432, 888–892.
- Jung, C., Voigt, S., Friedrich, O., Koch, M.C., Frank, M., 2013. Campanian–Maastrichtian ocean circulation in the tropical Pacific. *Paleoceanography* 28, 1–12, doi:10.1002/palo.20051.
- Kemp, D.B., Robinson, S.A., Crame, J.A., Francis, J.E., Ineson, J., Whittle, R.J., Vanessa Bowman, V., O’Brien, C., 2014. A cool temperate climate on the Antarctic Peninsula through the latest Cretaceous to early Paleogene. *Geology* 42, 583–586.
- Kidder, D.L., Worsley, T.R., 2012. A human-induced hot-house climate? *GSA Today* 22 (2), 4–11.
- Kump, L.R., Arthur, M.A., 1999. Interpreting carbon-isotope excursions; carbonates and organic matter. *Chemical Geology* 161, 181–198.
- Ladant, J.-B., Donnadieu, Y., 2016. Palaeogeographic regulation of glacial events during the Cretaceous supergreenhouse. *Nature Communications* 7, 12771, doi:10.1038/ncomms12771.
- Larson, R.L., 1991. Latest pulse of Earth: evidence for a mid–Cretaceous superplume. *Geology* 19, 547–550.
- Li, X., Jenkyns, H.C., Wang, C., Hu, X., Chen, X., Wei, Y., Huang, Y., Cui, J., 2006. Upper Cretaceous carbon- and oxygen-isotope stratigraphy of hemipelagic carbonate facies from southern Tibet, China. *Journal of the Geological Society*, 163, 375–382.
- Linnert, C., Robinson, S.A., Lees, J.A., Bown, P.R., Rodríguez, I.P., Petrizzo, M.R., Falzoni, F., Littler, K., Arz, J.A., Russell, E.E., 2014. Evidence for global cooling in the Late Cretaceous. *Nature Communications* 5, 4194, doi:10.1038/ncomms5194.
- MacLeod, K.G., Londoño, C.I., Martin, E.E., Jiménez Berrocoso, Á., Basak, C., 2011. Changes in North Atlantic circulation at the end of the Cretaceous greenhouse interval. *Nature Geoscience* 4, 779–782.
- MacLeod, K.G., Huber, B.T., Jiménez Berrocoso, Á., Wendler, I., 2013. A stable and hot Turonian without glacial $\delta^{18}\text{O}$ excursions is indicated by exquisitely preserved Tanzanian foraminifera. *Geology* 41, 1083–1086.
- Martin, E.E., MacLeod, K.G., Jiménez Berrocoso, Á., Bourbon, E., 2012. Water mass circulation on Demerara Rise during the Late Cretaceous based on Nd isotopes. *Earth and Planetary Science Letters* 327, 111–120.
- Miller, K.G., Barrera, E., Olsson, R.K., Sugarman, P.J., Savin, S.M., 1999. Does ice drive early Maastrichtian eustasy? *Geology* 27, 783–786.
- Miller, K.G., Wright, J.D., Browning, J.V., 2005. Visions of ice sheets in a greenhouse world. *Marine Geology* 217, 215–231.
- Moiroud, M., Pucéat, E., Donnadieu, Y., Bayon, G., Moriya, K., Deconinck, J.F., Boyet, M., 2013. Evolution of the neodymium isotopic signature of neritic seawater on a northwestern Pacific margin: new constraints on possible end-members for the composition of deep-water masses in the Late Cretaceous ocean. *Chemical Geology* 356, 160–170.
- Moiroud, M., Pucéat, E., Donnadieu, Y., Bayon, G., Guiraud, M., Voigt, S., Deconinck, J.F., Monna, F., 2016. Evolution of neodymium isotopic signature of seawater during the Late Cretaceous: Implications for intermediate and deep circulation. *Gondwana Research* 36, 503–522.
- Müller, R.D., Sdrolias, M., Gaina, C., Roest, W.R., 2008. Age, spreading rates, and spreading asymmetry of the world’s ocean crust. *Geochemistry, Geophysics, Geosystems* 9, Q04006, doi:10.1029/2007GC001743.
- Murphy, D.P., Thomas, D.J., 2012. Cretaceous deep-water formation in the Indian sector of the Southern Ocean. *Paleoceanography* 27, PA1211, doi:10.1029/2011PA002198.
- Murphy, D.P., Thomas, D.J., 2013. The evolution of Late Cretaceous deep-ocean circulation in the Atlantic basins:

- Neodymium isotope evidence from South Atlantic drill sites for tectonic controls. *Geochemistry, Geophysics, Geosystems* 14, 5323–5340, doi:10.1002/2013GC004889.
- Pérez-Rodríguez, I., Lees, J. A., Larrasoña, J. C., Arz, J. A., Arenillas, I., 2012. Planktonic foraminiferal and calcareous nannofossil biostratigraphy and magnetostratigraphy of the uppermost Campanian and Maastrichtian at Zumaia, northern Spain. *Cretaceous Research* 37, 100–126.
- Robinson, S. A., Murphy, D. P., Vance, D., Thomas, D. J., 2010. Formation of “Southern Component Water” in the Late Cretaceous: Evidence from Nd-isotopes. *Geology* 38, 871–874.
- Robinson, S. A., Vance, D., 2012. Widespread and synchronous change in deep-ocean circulation in the North and South Atlantic during the Late Cretaceous. *Paleoceanography* 27, doi:10.1029/2011PA002240.
- Sames, B., Wagreich, M., Wendler, J. E., Haq, B. U., Conrad, C. P., Melinte-Dobrinescu, M. C., Hu, X., Wendler, I., Wolfgring, E., Yilmaz, I. Ö., Zorina, S. O., 2016. Short-term sea-level changes in a greenhouse world – A view from the Cretaceous. *Palaeogeography, Palaeoclimatology, Palaeoecology* 441, 393–411.
- Sharp, Z., 2006. *Principles of Stable Isotope Geochemistry*. Prentice Hall, Upper Saddle River, New Jersey, 344 pp.
- Sinninghe Damsté, J. S., van Bentum, E. C., Reichert, G.-J., Pross, J., Schouten, S., 2010. A CO₂ decrease-driven cooling and increased latitudinal temperature gradient during the mid-Cretaceous Oceanic Anoxic Event 2. *Earth and Planetary Science Letters* 293, 91–103.
- Tabor, C. R., Poulsen, C. J., Lunt, D. J., Rosenbloom, N. A., Otto-Bliesner, B. L., Markwick, P. J., Brady, E. C., Farnsworth, A., Feng, R., 2016. The cause of Late Cretaceous cooling: A multi model-proxy Comparison. *Geology*, doi:10.1130/G38363.1
- Thibault, N., Harlou, R., Schovsbo, N., Schiøler, P., Minoletti, F., Galbrun, B., Lauridsen, B. W., Sheldon, E., Stemmerik, L., Surlyk, F., 2012a. Upper Campanian–Maastrichtian nannofossil biostratigraphy and high-resolution carbon-isotope stratigraphy of the Danish Basin: Towards a standard $\delta^{13}\text{C}$ curve for the Boreal Realm. *Cretaceous Research* 33, 72–90.
- Thibault, N., Husson, D., Harlou, R., Gardin, S., Galbrun, B., Huret, E., Minoletti, F., 2012b. Astronomical calibration of upper Campanian–Maastrichtian carbon isotope events and calcareous plankton biostratigraphy in the Indian Ocean (ODP Hole 762C): Implication for the age of the Campanian–Maastrichtian boundary. *Palaeogeography, Palaeoclimatology, Palaeoecology* 337–338, 52–71.
- Veizer, 1983. Chemical diagenesis of carbonates: theory and application of trace element technique. In: Arthur, M. A., Anderson, T. F., Kaplan, I. R., Veizer, J., Land, L. S. (Eds.), *Stable Isotopes in Sedimentary Geology: Society of Economic Paleontologists and Mineralogists Short Course No. 10*. Dallas, pp. 3/1–3/10.
- Voigt, S., Friedrich, O., Norris, R. D., Schönfeld, J., 2010. Campanian–Maastrichtian carbon isotope stratigraphy: shelf-ocean correlation between the European shelf sea and the tropical Pacific Ocean. *Newsletters on Stratigraphy* 44, 57–72.
- Voigt, S., Gale, A. S., Jung, C., Jenkyns, H. C., 2012. Global correlation of Upper Campanian–Maastrichtian successions using carbon-isotope stratigraphy: development of a new Maastrichtian timescale. *Newsletters on Stratigraphy* 45, 25–53.
- Voigt, S., Jung, C., Friedrich, O., Frank, M., Teschner, C., Hoffmann, J., 2013. Tectonically restricted deep-ocean circulation at the end of the Cretaceous greenhouse. *Earth and Planetary Science Letters* 369–370, 169–177.
- Wagreich, M., Lein, R., Sames, B., 2014. Eustasy, its controlling factors, and the limno-eustatic hypothesis – concepts inspired by Eduard Suess. *Journal of Austrian Earth Sciences* 107, 115–131.
- Wendler, I., 2013. A critical evaluation of carbon isotope stratigraphy and biostratigraphic implications for Late Cretaceous global correlation. *Earth Science Reviews* 126, 116–146.
- Wendler, J. E., Wendler, I. 2016. What drove cyclic sea-level fluctuations during the mid-Cretaceous greenhouse climate? *Palaeogeography, Palaeoclimatology, Palaeoecology* 441, 412–419.
- Wendler I., Willems, H., Gräfe, K.-U., Ding, L., Luo, H., 2011. Upper Cretaceous inter-hemispheric correlation between the Southern Tethys and the Boreal: chemo- and biostratigraphy and paleoclimatic reconstructions from a new section in the Tethys Himalaya, S-Tibet. *Newsletters on Stratigraphy* 44, 137–171.
- Wilson, P. A., Norris, R. D., Cooper, M. J., 2002. Testing the Cretaceous greenhouse hypothesis using glassy foraminiferal calcite from the core of the Turonian tropics on Demerara Rise. *Geology* 30, 607–610.
- Zachos, J. C., Dickens, G. R., Zeebe, R. E., 2008. An early Cenozoic perspective on greenhouse warming and carbon-cycle dynamics. *Nature* 451, 279–283.

Manuscript received: January 4, 2016

Revised version accepted: March 17, 2017

Appendices

Supplementary Table 1 Geochemical data from the Shuqualak-Evans core (TOC, %CaCO₃, δ¹³C_{carbonate}, δ¹⁸O_{carbonate}).

Sample Name	Depth (m)	Age (Ma) <small>after Linneert et al. 2014</small>	Age (Ma) <small>this study</small>	δ ¹³ C	δ ¹⁸ O	CaCO ₃ (%)	TOC (%)	Sample Name	Depth (m)	Age (Ma) <small>after this Linneert et al. 2014</small>	Age (Ma) <small>this study</small>	δ ¹³ C	δ ¹⁸ O	CaCO ₃ (%)	TOC (%)
SHUQ31	9.45	65.71	65.71	0.77	−2.11	69.8	0.35	SHUQ280	85.34	75.86	75.86	1.45	−2.42	79.8	0.41
SHUQ36	10.97	66.43	66.43	0.86	−2.46	85.8	0.20	SHUQ285	86.87	75.91	75.91	1.62	−2.24	82.0	0.39
SHUQ42	12.80	67.30	67.30	0.96	−1.94	74.9	0.37	SHUQ290	88.39	75.97	75.97	1.50	−2.43	81.3	0.45
SHUQ45	13.72	67.73	67.74	0.74	−2.31	71.5	0.27	SHUQ295	89.92	76.02	76.02	1.38	−2.22	84.2	0.32
SHUQ50	15.24	68.46	68.46	0.21	−1.71	69.8	0.31	SHUQ300	91.44	76.08	76.08	1.52	−2.10	74.8	0.65
SHUQ55	16.76	69.18	69.18	0.85	−1.84	69.4	0.39	SHUQ304.5	92.81	76.13	76.13	1.07	−1.91	79.9	0.50
SHUQ60	18.29	69.91	69.50	0.93	−1.34	48.4	0.42	SHUQ305	92.96	76.13	76.13	1.19	−2.00	79.7	0.58
SHUQ65	19.81	70.63	69.82	1.03	−1.32	56.6	0.46	SHUQ310	94.49	76.19	76.19	1.13	−2.05	80.0	0.49
SHUQ70	21.34	71.35	70.14	0.48	−1.63	73.2	0.38	SHUQ315	96.01	76.24	76.24	1.16	−1.77	81.9	0.55
SHUQ75	22.86	72.08	70.46	0.89	−1.57	67.4	0.36	SHUQ320	97.54	76.30	76.30	1.32	−2.10	89.9	0.29
SHUQ80	24.38	72.80	70.78	0.45	−1.63	62.2	0.29	SHUQ325	99.06	76.35	76.35	1.36	−2.17	80.5	0.46
SHUQ85	25.91	73.52	71.10	1.19	−1.65	38.1	0.51	SHUQ330	100.58	76.41	76.41	1.23	−2.26	84.5	0.33
SHUQ90	27.43	73.78	71.42	0.22	−1.92	24.2	0.58	SHUQ335	102.11	76.46	76.46	1.49	−2.01	73.8	0.67
SHUQ95	28.96	73.83	71.62	0.99	−1.71	59.8	0.31	SHUQ340	103.63	76.52	76.52	1.40	−2.38	84.4	0.41
SHUQ100	30.48	73.89	71.74	0.23	−2.28	51.9	0.37	SHUQ345	105.16	76.57	76.57	1.32	−2.29	87.4	0.39
SHUQ105	32.00	73.94	71.86	0.54	−2.19	52.9	0.34	SHUQ350	106.68	76.62	76.62	1.30	−2.27	86.0	0.42
SHUQ110	33.53	74.00	71.97	1.00	−1.40	44.5	0.60	SHUQ355	108.20	76.68	76.68	1.32	−1.94	79.2	0.56
SHUQ115	35.05	74.05	72.09	0.64	−2.15	55.5	0.48	SHUQ360	109.73	76.73	76.73	1.40	−2.38	80.2	0.59
SHUQ120	36.58	74.11	72.21	0.78	−2.01	42.3	0.57	SHUQ365	111.25	76.79	76.79	1.45	−2.12	78.0	0.83
SHUQ125	38.10	74.16	72.32	1.25	−1.77	37.1	0.54	SHUQ370	112.78	76.84	76.84	1.30	−2.38	74.9	0.67
SHUQ130	39.62	74.22	72.44	0.31	−2.97	64.4	0.43	SHUQ375	114.30	76.90	76.90	1.24	−2.48	79.5	0.63
SHUQ135	41.15	74.27	72.56	0.95	−2.06	64.5	0.35	SHUQ380	115.82	76.95	76.95	1.40	−2.26	62.3	1.14
SHUQ140	42.67	74.33	72.67	0.73	−1.87	51.9	0.45	SHUQ385	117.35	77.01	77.01	1.54	−2.17	57.2	1.28
SHUQ145	44.20	74.38	72.79	1.30	−1.85	47.1	0.51	SHUQ390	118.87	77.06	77.06	1.37	−2.39	67.1	0.84
SHUQ149	45.42	74.43	72.88	1.32	−1.58	40.0	0.63	SHUQ395	120.40	77.12	77.12	0.99	−2.43	72.1	0.57
SHUQ150	45.72	74.44	72.91	1.38	−2.08	47.9	0.51	SHUQ400	121.92	77.17	77.17	1.28	−2.47	72.4	0.86
SHUQ154	46.94	74.48	73.00	1.38	−1.48	46.5	0.50	SHUQ420	128.02	77.39	77.39	1.23	−2.42	67.3	0.94
SHUQ155	47.24	74.49	73.02	1.09	−2.00	68.4	0.32	SHUQ425	129.54	77.45	77.45	1.07	−2.58	77.1	0.68
SHUQ160	48.77	74.55	73.14	1.02	−1.60	74.0	0.30	SHUQ430	131.06	77.50	77.50	1.21	−2.67	74.7	0.69
SHUQ165	50.29	74.60	73.26	1.21	−1.92	73.1	0.30	SHUQ435	132.59	77.55	77.55	1.10	−2.45	74.6	0.56
SHUQ170	51.82	74.66	73.37	1.08	−1.77	80.6	0.28	SHUQ440	134.11	77.61	77.61	1.11	−3.08	69.1	0.53
SHUQ175	53.34	74.71	73.49	1.31	−1.99	86.2	0.21	SHUQ445	135.64	77.66	77.66	1.18	−2.43	68.4	0.72
SHUQ180	54.86	74.76	73.61	1.48	−1.64	83.8	0.24	SHUQ450	137.16	77.72	77.72	1.24	−2.60	63.5	0.62
SHUQ185	56.39	74.82	73.72	1.43	−1.87	88.1	0.16	SHUQ455	138.68	77.77	77.77	1.43	−2.32	59.2	0.93
SHUQ190	57.91	74.87	73.84	1.30	−1.75	84.0	0.24	SHUQ460	140.21	77.83	77.83	1.70	−2.40	49.1	1.36
SHUQ195	59.44	74.93	73.96	1.39	−1.69	89.6	0.20	SHUQ465	141.73	77.88	77.88	1.61	−2.43	51.7	1.28
SHUQ200	60.96	74.98	74.07	1.41	−1.93	86.9	0.21	SHUQ470	143.26	77.94	77.94	1.52	−2.48	66.5	1.05
SHUQ205	62.48	75.04	74.19	1.49	−1.63	80.4	0.27	SHUQ475	144.78	77.99	77.99	1.39	−2.65	70.1	0.81
SHUQ210	64.01	75.09	74.31	1.30	−2.19	80.4	0.28	SHUQ480	146.30	78.05	78.05	1.71	−2.19	62.4	1.18
SHUQ215	65.53	75.15	74.42	1.41	−1.87	86.2	0.19	SHUQ485	147.83	78.10	78.10	1.13	−2.77	72.4	0.63
SHUQ220	67.06	75.20	74.54	1.44	−1.95	90.3	0.18	SHUQ490	149.35	78.16	78.16	1.93	−2.47	48.7	0.91
SHUQ225	68.58	75.26	74.66	1.53	−1.83	85.0	0.24	SHUQ495	150.88	78.21	78.21	1.31	−2.67	72.9	0.57
SHUQ230	70.10	75.31	74.78	1.50	−1.99	81.9	0.33	SHUQ500	152.40	78.27	78.27	1.42	−2.79	73.9	0.95
SHUQ235	71.63	75.37	74.89	1.39	−2.02	82.8	0.37	SHUQ505	153.92	78.32	78.32	1.49	−2.73	58.6	0.73
SHUQ240	73.15	75.42	75.01	1.45	−2.42	82.3	0.39	SHUQ510	155.45	78.38	78.38	1.27	−2.87	76.9	0.61
SHUQ245	74.68	75.48	75.13	1.45	−2.43	79.9	0.32	SHUQ515	156.97	78.43	78.43	1.66	−2.60	55.3	1.51
SHUQ250	76.20	75.53	75.24	1.46	−2.46	79.0	0.31	SHUQ520	158.50	78.49	78.49	1.30	−2.76	69.7	0.75
SHUQ255	77.72	75.59	75.36	1.55	−2.69	81.8	0.34	SHUQ525	160.02	78.54	78.54	1.24	−2.74	65.6	0.75
SHUQ260	79.25	75.64	75.48	1.50	−2.73	78.3	0.41	SHUQ530	161.54	78.59	78.59	1.54	−2.50	60.8	1.29
SHUQ265	80.77	75.69	75.59	1.72	−2.39	71.2	0.48	SHUQ535	163.07	78.65	78.65	1.47	−2.38	55.2	1.26
SHUQ270	82.30	75.75	75.71	1.71	−2.46	67.1	0.46	SHUQ540	164.59	78.70	78.70	1.01	−2.75	60.7	1.05
SHUQ275	83.82	75.80	75.80	1.32	−2.36	81.9	0.39	SHUQ545	166.12	78.76	78.76	0.97	−2.40	64.4	0.91

Sample Name	Depth (m)	Age (Ma) <small>after Linneert et al. 2014</small>	Age (Ma) <small>this study</small>	$\delta^{13}\text{C}$	$\delta^{18}\text{O}$	CaCO_3 (%)	TOC (%)
SHUQ550	167.64	78.81	78.81	1.19	-3.20	62.3	1.15
SHUQ555	169.16	78.87	78.87	1.06	-3.53	67.3	0.86
SHUQ560	170.69	78.92	78.92	1.65	-2.33	43.6	1.41
SHUQ565	172.21	78.98	78.98	1.39	-3.17	56.9	1.04
SHUQ570	173.74	79.03	79.03	1.32	-2.69	60.2	0.71
SHUQ575	175.26	79.09	79.09	1.84	-2.86	86.8	0.57
SHUQ580	176.78	79.14	79.14	1.66	-2.80	67.6	0.47
SHUQ585	178.31	79.20	79.20	0.66	-2.63	66.6	0.40
SHUQ590	179.83	79.25	79.25	1.50	-2.78	56.1	0.81
SHUQ595	181.36	79.31	79.31	1.40	-2.74	43.8	1.06
SHUQ600	182.88	79.36	79.36	1.45	-3.07	59.2	0.89
SHUQ605	184.40	79.42	79.42	1.26	-2.76	72.3	0.87
SHUQ610	185.93	79.47	79.47	1.31	-3.12	51.8	1.08
SHUQ615	187.45	79.52	79.52	0.84	-2.65	53.6	1.00
SHUQ630	192.02	79.69	79.69	1.03	-3.21	48.7	1.17
SHUQ633	192.94	79.72	79.72	n.a.	n.a.	0.0	0.17
SHUQ635	193.55	79.74	79.74	1.03	-3.19	56.8	1.17
SHUQ640	195.07	79.80	79.80	0.85	-2.82	54.7	1.50
SHUQ645	196.60	79.85	79.85	1.38	-3.07	62.4	1.17
SHUQ650	198.12	79.91	79.91	0.65	-2.74	61.2	0.63
SHUQ655	199.64	79.96	79.96	1.08	-2.87	58.3	0.76
SHUQ660	201.17	80.02	80.02	0.84	-3.02	56.3	1.46
SHUQ665	202.69	80.07	80.07	1.44	-2.92	61.1	1.05
SHUQ670	204.22	80.13	80.13	0.93	-2.56	61.9	1.09
SHUQ675	205.74	80.18	80.18	0.78	-2.80	63.2	0.75
SHUQ680	207.26	80.24	80.24	0.95	-3.06	65.8	1.50
SHUQ685	208.79	80.29	80.29	1.12	-3.20	68.2	1.17
SHUQ690	210.31	80.35	80.35	0.89	-3.03	61.9	1.45

Sample Name	Depth (m)	Age (Ma) <small>after Linneert et al. 2014</small>	Age (Ma) <small>this study</small>	$\delta^{13}\text{C}$	$\delta^{18}\text{O}$	CaCO_3 (%)	TOC (%)
SHUQ695	211.84	80.40	80.40	0.54	-3.05	75.7	0.50
SHUQ700	213.36	80.45	80.45	0.87	-2.82	67.7	1.02
SHUQ705	214.88	80.51	80.51	1.01	-3.56	58.3	1.43
SHUQ710	216.41	80.56	80.56	1.30	-3.08	54.3	1.49
SHUQ715	217.93	80.62	80.62	1.32	-3.08	60.4	0.99
SHUQ720	219.46	80.67	80.67	0.85	-2.68	69.1	0.91
SHUQ725	220.98	80.73	80.73	1.33	-3.41	43.1	0.51
SHUQ740	225.55	80.89	80.89	1.25	-2.92	67.3	1.05
SHUQ745	227.08	80.95	80.95	1.28	-3.27	70.6	1.10
SHUQ750	228.60	81.00	81.00	1.16	-3.31	67.0	1.24
SHUQ755	230.12	81.06	81.06	0.86	-2.96	69.5	0.73
SHUQ760	231.65	81.11	81.11	0.89	-3.63	68.1	1.16
SHUQ765	233.17	81.17	81.17	1.17	-3.65	69.1	1.02
SHUQ770	234.70	81.22	81.22	0.98	-3.63	74.1	1.02
SHUQ775	236.22	81.28	81.28	0.95	-3.19	66.7	1.10
SHUQ780	237.74	81.33	81.33	1.53	-3.05	56.7	0.59
SHUQ785	239.27	81.38	81.38	1.09	-2.98	79.8	0.53
SHUQ790	240.79	81.44	81.44	0.95	-2.96	68.0	0.81
SHUQ795	242.32	81.49	81.49	0.95	-3.64	71.1	0.62
SHUQ800	243.84	81.55	81.55	1.18	-2.77	54.1	0.92
SHUQ805	245.36	81.60	81.60	1.25	-3.22	65.2	0.79
SHUQ810	246.89	81.66	81.66	1.05	-3.24	64.6	0.83
SHUQ815	248.41	81.71	81.71	1.67	-3.36	26.9	0.41
SHUQ820	249.94	82.00	81.77	1.41	-2.99	38.5	0.69
SHUQ825	251.46	82.56	83.02	1.10	-3.28	43.6	0.50
SHUQ826.67	251.97	82.75	83.20	n.a.	n.a.	31.7	0.69
SHUQ829.5	252.83	83.07	83.51	-1.42	-5.82	16.2	0.36
SHUQ830.67	253.19	83.20	83.64	n.a.	n.a.	0.4	0.28

Supplementary Table 2 Stable-isotope data ($\delta^{13}\text{C}_{\text{carbonate}}$, $\delta^{18}\text{O}_{\text{carbonate}}$) from the Trunch core.

Depth (m)	Age (Ma)	$\delta^{13}\text{C}$	$\delta^{18}\text{O}$	Depth (m)	Age (Ma)	$\delta^{13}\text{C}$	$\delta^{18}\text{O}$	Depth (m)	Age (Ma)	$\delta^{13}\text{C}$	$\delta^{18}\text{O}$
47.17	72.45	1.68	−1.77	101.60	74.43	1.98	−1.84	111.00	75.02	1.95	−1.75
48.10	72.47	1.68	−1.89	101.70	74.44	2.03	−1.84	111.07	75.02	2.02	−1.94
49.00	72.50	1.76	−1.77	101.80	74.45	2.09	−1.96	111.10	75.03	1.95	−1.68
49.78	72.52	1.72	−1.77	102.00	74.46	2.10	−1.64	111.20	75.03	1.98	−1.76
58.00	72.75	1.89	−2.31	102.10	74.47	2.08	−1.76	111.31	75.04	1.94	−1.98
58.98	72.77	1.95	−2.03	102.11	74.47	1.91	−1.87	111.40	75.04	1.97	−2.05
60.10	72.80	1.99	−2.11	102.20	74.47	2.01	−1.83	111.50	75.05	2.01	−1.81
61.00	72.83	1.93	−1.99	102.30	74.48	2.04	−1.84	111.60	75.06	1.92	−1.95
62.53	72.87	2.04	−2.02	102.40	74.48	1.97	−1.87	111.70	75.06	1.97	−1.81
64.00	72.92	1.92	−2.08	102.50	74.49	2.18	−1.13	111.80	75.07	1.95	−1.51
67.51	73.08	1.93	−2.27	102.60	74.50	2.07	−1.65	111.86	75.07	1.96	−1.62
71.13	73.25	2.00	−1.81	102.70	74.50	1.97	−1.77	111.90	75.08	1.97	−1.84
80.45	73.56	1.90	−2.43	102.80	74.51	1.93	−1.85	112.00	75.08	2.03	−1.73
81.10	73.57	1.99	−2.35	103.00	74.52	2.03	−1.71	112.10	75.09	1.95	−1.70
82.28	73.61	1.89	−1.89	103.01	74.52	2.04	−1.71	112.20	75.09	1.95	−1.74
83.11	73.63	1.94	−2.16	103.10	74.53	2.01	−1.86	112.20	75.09	1.91	−1.88
84.00	73.65	2.03	−1.90	103.20	74.53	2.08	−1.68	112.30	75.10	1.91	−1.78
85.15	73.68	2.07	−1.87	104.01	74.58	2.06	−1.86	112.40	75.11	1.98	−1.70
86.35	73.71	1.99	−1.94	104.10	74.59	2.06	−1.65	112.50	75.11	1.98	−1.56
87.15	73.74	2.09	−2.00	104.20	74.60	2.10	−1.69	112.60	75.12	2.00	−1.65
88.12	73.76	2.15	−1.98	104.20	74.60	2.08	−1.70	112.70	75.13	2.01	−1.73
89.59	73.80	2.09	−1.95	104.30	74.60	2.04	−1.85	112.80	75.13	1.98	−1.65
90.33	73.82	2.15	−1.89	104.40	74.61	1.95	−1.76	112.90	75.14	2.02	−1.66
90.85	73.84	2.04	−1.81	104.50	74.62	1.97	−1.78	113.00	75.14	2.03	−1.54
92.20	73.88	2.04	−1.88	104.60	74.62	2.00	−1.79	113.10	75.15	1.98	−1.62
93.10	73.93	1.94	−1.69	105.63	74.69	1.88	−2.02	113.20	75.16	2.00	−1.79
94.40	74.00	2.13	−1.79	105.70	74.69	2.04	−1.87	113.28	75.16	1.97	−1.60
95.12	74.03	2.02	−1.95	106.00	74.71	1.98	−1.71	113.30	75.16	1.96	−1.53
96.00	74.09	2.03	−1.97	106.20	74.72	2.03	−1.98	113.40	75.17	1.96	−1.62
97.05	74.15	2.13	−1.77	106.30	74.73	1.92	−1.64	113.50	75.18	1.94	−1.71
98.25	74.23	2.09	−1.83	106.60	74.75	2.03	−1.73	113.60	75.18	1.96	−1.80
99.20	74.29	2.15	−1.85	106.70	74.75	2.02	−1.77	113.70	75.19	1.98	−1.82
99.28	74.29	2.02	−1.78	106.80	74.76	2.07	−1.79	113.79	75.19	1.88	−1.84
99.30	74.29	2.07	−1.79	108.40	74.86	2.05	−1.79	113.90	75.20	1.93	−1.79
99.40	74.30	2.04	−1.92	108.84	74.89	1.88	−1.97	114.05	75.21	1.94	−1.74
99.50	74.30	2.08	−1.87	108.91	74.89	1.90	−1.96	114.10	75.21	1.97	−1.74
99.60	74.31	1.99	−1.75	109.00	74.90	1.85	−1.72	114.20	75.22	1.99	−1.71
99.70	74.32	2.09	−1.34	109.09	74.90	1.87	−1.88	114.30	75.22	1.98	−1.85
99.80	74.32	2.00	−1.88	109.10	74.90	1.90	−1.79	114.39	75.23	1.94	−1.76
99.90	74.33	2.01	−1.55	109.20	74.91	1.87	−1.74	114.50	75.24	1.87	−1.79
100.00	74.33	2.05	−1.36	109.30	74.91	1.90	−1.79	114.60	75.24	1.97	−1.64
100.10	74.34	2.07	−1.86	109.40	74.92	1.98	−1.74	114.70	75.25	1.95	−1.74
100.20	74.35	2.07	−1.67	109.50	74.93	1.91	−1.61	114.80	75.26	1.90	−1.75
100.20	74.35	2.03	−1.76	109.60	74.93	2.05	−1.92	114.90	75.26	1.93	−1.84
100.30	74.35	2.07	−1.83	109.70	74.94	2.03	−2.05	115.06	75.27	2.01	−1.60
100.40	74.36	2.08	−1.79	109.80	74.94	2.05	−2.00	115.10	75.27	1.89	−1.77
100.50	74.37	2.06	−1.67	109.90	74.95	2.08	−1.98	115.20	75.28	1.89	−1.53
100.60	74.37	2.06	−1.82	110.00	74.96	2.08	−1.88	115.30	75.29	1.83	−1.82
100.70	74.38	2.04	−1.84	110.00	74.96	2.03	−1.72	115.40	75.29	1.87	−1.93
100.80	74.38	2.05	−1.87	110.10	74.96	2.10	−1.77	115.50	75.30	1.85	−2.11
100.90	74.39	2.11	−1.74	110.20	74.97	2.02	−1.80	115.60	75.31	1.82	−1.64
101.00	74.40	2.12	−1.77	110.30	74.98	2.05	−1.90	115.70	75.31	1.76	−1.99
101.10	74.40	1.99	−1.91	110.40	74.98	2.01	−1.80	115.80	75.32	1.76	−1.99
101.10	74.40	2.03	−1.62	110.50	74.99	1.96	−1.73	115.90	75.32	1.73	−1.97
101.20	74.41	2.11	−1.68	110.60	74.99	1.98	−1.63	116.10	75.34	1.79	−1.91
101.30	74.42	2.05	−1.74	110.70	75.00	2.04	−1.62	116.20	75.34	1.79	−2.00
101.40	74.42	1.95	−1.84	110.80	75.01	2.01	−1.65	116.25	75.35	1.75	−2.04
101.50	74.43	2.03	−1.65	110.90	75.01	1.94	−1.90	116.30	75.35	1.78	−2.09

Depth (m)	Age (Ma)	$\delta^{13}\text{C}$	$\delta^{18}\text{O}$	Depth (m)	Age (Ma)	$\delta^{13}\text{C}$	$\delta^{18}\text{O}$	Depth (m)	Age (Ma)	$\delta^{13}\text{C}$	$\delta^{18}\text{O}$
116.40	75.36	1.79	-2.13	129.50	75.81	1.93	-1.62	136.60	76.04	1.94	-1.78
116.50	75.36	1.81	-1.86	129.60	75.81	2.00	-1.87	136.70	76.04	2.03	-1.83
116.60	75.37	1.78	-1.90	129.70	75.81	1.98	-1.78	136.80	76.04	1.95	-1.84
116.70	75.37	1.88	-1.99	129.80	75.82	2.05	-1.36	136.90	76.05	1.94	-2.34
116.80	75.38	1.78	-2.03	129.90	75.82	1.98	-1.71	137.00	76.05	1.98	-1.87
116.90	75.39	1.69	-1.74	130.00	75.82	1.88	-1.69	137.00	76.05	2.02	-1.77
117.00	75.39	1.83	-1.78	130.10	75.83	1.87	-1.87	137.10	76.05	2.01	-1.74
122.20	75.56	1.63	-1.84	130.10	75.83	1.95	-1.87	137.20	76.06	1.92	-1.82
122.45	75.57	1.73	-1.82	130.20	75.83	1.92	-1.76	137.30	76.06	1.91	-1.77
122.45	75.57	1.46	-2.02	130.30	75.83	1.99	-1.73	137.40	76.06	1.97	-1.64
124.00	75.62	1.41	-1.73	130.40	75.84	1.98	-1.86	137.50	76.07	2.04	-1.91
124.10	75.63	1.52	-2.04	130.50	75.84	1.96	-1.63	137.60	76.07	2.04	-2.01
124.26	75.63	1.59	-1.83	130.60	75.84	2.00	-1.66	137.70	76.07	1.93	-2.02
124.40	75.64	1.65	-2.38	130.70	75.85	2.02	-1.81	137.80	76.08	2.08	-1.73
124.42	75.64	1.59	-1.96	130.80	75.85	2.03	-2.01	137.90	76.08	2.04	-2.09
124.50	75.64	1.67	-1.94	130.90	75.85	2.01	-2.09	138.00	76.09	2.15	-1.94
124.60	75.64	1.68	-1.72	131.02	75.86	2.00	-1.63	138.10	76.09	2.10	-1.89
124.70	75.65	1.66	-1.92	131.06	75.86	1.93	-1.84	138.20	76.09	2.01	-2.01
124.80	75.65	1.77	-2.03	131.20	75.86	2.02	-1.75	138.30	76.10	2.06	-1.83
124.90	75.65	1.71	-2.12	131.30	75.87	2.01	-1.79	138.40	76.10	2.25	-1.38
125.00	75.66	1.60	-2.18	131.40	75.87	2.03	-1.91	138.50	76.10	2.12	-1.49
125.00	75.66	1.74	-2.03	131.50	75.87	2.02	-1.85	138.60	76.11	2.16	-1.94
125.10	75.66	1.69	-2.19	131.60	75.88	2.09	-1.81	138.70	76.11	2.22	-1.90
125.20	75.66	1.76	-1.75	131.70	75.88	2.03	-1.80	138.80	76.11	2.11	-2.34
125.30	75.67	1.64	-1.74	131.80	75.88	2.06	-1.80	138.90	76.12	2.15	-1.81
125.40	75.67	1.87	-1.78	131.90	75.89	1.99	-1.88	139.40	76.13	2.22	-1.89
125.60	75.68	1.91	-1.89	132.00	75.89	2.10	-1.77	139.50	76.14	2.12	-1.78
125.70	75.68	1.89	-1.95	132.00	75.89	2.03	-2.00	139.60	76.14	2.05	-1.85
125.80	75.68	1.89	-2.26	132.10	75.89	1.99	-1.82	139.70	76.14	2.02	-1.88
125.90	75.69	1.84	-2.25	132.20	75.90	2.08	-1.74	139.80	76.15	2.07	-1.85
126.00	75.69	1.59	-2.08	132.30	75.90	2.06	-1.73	139.90	76.15	2.08	-1.62
126.00	75.69	1.91	-2.26	132.40	75.90	2.10	-1.82	140.00	76.16	2.08	-1.72
126.10	75.69	1.94	-1.67	132.50	75.91	2.06	-1.83	140.10	76.16	2.08	-1.64
126.20	75.70	1.86	-1.79	132.60	75.91	2.07	-1.91	140.20	76.16	2.09	-1.68
126.30	75.70	1.85	-1.82	132.70	75.91	2.08	-1.63	140.30	76.17	2.09	-1.61
126.40	75.70	1.94	-1.84	132.74	75.91	2.09	-1.73	140.40	76.17	2.10	-1.58
126.50	75.71	1.93	-1.79	133.20	75.93	2.08	-1.62	140.50	76.17	2.10	-1.73
126.60	75.71	1.92	-1.98	133.25	75.93	2.05	-1.83	140.60	76.18	2.08	-1.81
126.70	75.71	1.82	-1.85	133.30	75.93	2.08	-1.66	140.70	76.18	2.09	-1.69
126.80	75.72	1.76	-1.96	133.40	75.94	2.14	-1.62	140.80	76.18	2.14	-1.70
126.90	75.72	1.96	-0.92	133.50	75.94	2.10	-1.61	140.90	76.19	2.16	-1.67
127.00	75.72	1.78	-1.75	133.60	75.94	2.04	-1.67	141.00	76.19	2.25	-1.87
127.05	75.73	1.76	-1.69	133.70	75.95	1.97	-1.89	141.00	76.19	2.12	-1.75
127.10	75.73	1.71	-1.92	133.80	75.95	2.04	-1.67	141.10	76.19	2.07	-1.77
127.20	75.73	1.82	-1.74	133.90	75.95	2.01	-1.88	141.20	76.20	2.17	-1.69
127.30	75.73	1.81	-1.85	134.00	75.95	2.15	-1.85	141.30	76.20	2.11	-1.80
128.12	75.76	1.86	-1.78	134.00	75.96	2.16	-1.49	141.40	76.20	2.15	-1.84
128.15	75.76	1.89	-1.89	134.10	75.96	2.09	-1.90	141.50	76.21	2.08	-2.38
128.20	75.76	1.84	-1.74	135.53	76.01	1.97	-2.06	141.60	76.21	2.07	-2.30
128.30	75.77	2.01	-1.87	135.60	76.01	2.10	-1.87	141.70	76.22	2.15	-1.81
128.60	75.78	1.90	-1.61	135.60	76.01	2.00	-1.91	141.80	76.22	2.07	-1.82
128.70	75.78	1.89	-1.77	135.70	76.01	2.03	-1.88	141.90	76.22	2.12	-1.58
128.80	75.78	1.84	-1.69	135.80	76.01	2.06	-1.78	142.00	76.23	2.08	-1.80
128.90	75.79	1.86	-2.04	135.90	76.02	2.13	-1.24	142.10	76.23	2.11	-1.67
129.00	75.79	1.86	-1.78	136.00	76.02	2.05	-1.82	142.20	76.23	2.12	-1.76
129.10	75.79	1.87	-1.76	136.10	76.02	2.06	-1.67	142.20	76.23	2.14	-1.81
129.12	75.79	1.88	-1.90	136.20	76.03	1.99	-1.85	142.30	76.24	2.12	-1.83
129.20	75.80	1.91	-1.79	136.30	76.03	2.02	-1.75	142.40	76.24	2.09	-1.88
129.30	75.80	1.87	-1.75	136.40	76.03	2.04	-1.96	142.50	76.25	2.15	-1.76
129.40	75.80	1.94	-1.66	136.50	76.04	1.96	-1.70	142.60	76.25	2.14	-1.90

Depth (m)	Age (Ma)	$\delta^{13}\text{C}$	$\delta^{18}\text{O}$	Depth (m)	Age (Ma)	$\delta^{13}\text{C}$	$\delta^{18}\text{O}$	Depth (m)	Age (Ma)	$\delta^{13}\text{C}$	$\delta^{18}\text{O}$
142.70	76.25	2.17	−2.05	148.90	76.48	2.11	−1.65	194.25	78.31	2.38	−2.09
142.80	76.26	2.16	−1.98	149.00	76.49	2.11	−1.85	195.05	78.34	2.43	−2.03
142.90	76.26	2.18	−1.97	149.10	76.49	2.18	−1.63	199.06	78.49	2.55	−1.89
143.00	76.26	2.19	−2.14	149.20	76.49	2.18	−1.82	199.99	78.53	2.55	−2.06
143.10	76.27	2.18	−1.77	149.30	76.50	2.13	−1.86	201.29	78.58	2.54	−2.07
143.17	76.27	2.14	−1.73	149.40	76.50	2.13	−1.88	202.14	78.61	2.45	−1.99
143.20	76.27	2.10	−2.18	149.40	76.50	2.17	−1.76	204.76	78.71	2.55	−2.03
143.30	76.28	2.26	−1.73	149.50	76.50	2.15	−1.71	205.32	78.73	2.56	−2.00
143.30	76.28	2.16	−1.99	149.60	76.51	2.22	−1.81	206.51	78.77	2.48	−1.87
143.40	76.28	2.20	−2.04	149.70	76.51	2.16	−1.87	207.36	78.81	2.50	−2.12
143.50	76.28	2.18	−2.01	149.80	76.52	2.20	−2.13	208.24	78.84	2.55	−1.99
143.60	76.29	2.18	−2.15	149.90	76.52	2.21	−2.06	209.07	78.87	2.54	−2.05
143.70	76.29	2.21	−2.05	150.00	76.52	2.21	−1.92	209.19	78.88	2.52	−2.21
143.80	76.29	2.19	−1.97	150.10	76.53	2.14	−2.10	211.00	78.94	2.42	−2.21
143.90	76.30	2.17	−1.90	150.10	76.53	2.15	−1.84	212.24	78.99	2.19	−1.99
144.00	76.30	2.18	−2.40	150.20	76.53	2.13	−1.92	213.20	79.04	2.40	−2.10
144.10	76.30	2.15	−1.90	150.30	76.53	2.19	−1.85	214.00	79.07	2.33	−2.10
144.10	76.30	2.16	−2.31	150.40	76.54	2.21	−1.81	215.14	79.13	2.46	−2.11
144.20	76.31	2.26	−2.06	150.50	76.54	2.22	−1.94	215.97	79.17	2.47	n.a.
144.30	76.31	2.27	−2.18	152.00	76.60	2.19	−1.87	217.25	79.23	2.42	−2.12
144.40	76.32	2.17	−2.24	152.05	76.60	2.22	−2.03	218.14	79.27	2.33	−2.09
144.50	76.32	2.17	−1.89	152.10	76.60	2.18	−1.71	219.23	79.32	2.53	−2.09
144.60	76.32	2.16	−1.96	152.20	76.60	2.13	−1.87	220.05	79.36	2.38	−2.45
144.70	76.33	2.16	−1.94	152.30	76.61	2.09	−2.07	221.10	79.41	2.52	−2.14
144.80	76.33	2.23	−1.89	156.37	76.76	2.18	−1.87	222.05	79.45	2.61	−2.25
144.90	76.33	2.17	−1.93	157.13	76.79	2.13	−2.00	223.00	79.50	2.35	−2.31
145.00	76.34	2.19	−2.04	159.15	76.86	2.20	−2.08	225.15	79.60	2.48	−2.23
145.10	76.34	2.14	−2.11	160.16	76.90	2.08	−1.91	226.10	79.64	2.48	−2.23
145.18	76.34	2.24	−2.07	161.00	76.93	2.24	−2.05	227.10	79.69	2.46	−2.09
145.20	76.35	2.18	−2.28	162.33	76.98	2.25	−1.88	228.06	79.74	2.37	−2.14
145.30	76.35	2.18	−2.20	163.68	77.03	2.24	−2.12	229.06	79.78	2.47	−2.28
145.40	76.35	2.19	−2.15	164.05	77.04	2.27	−1.93	230.00	79.83	2.45	−2.44
145.50	76.36	2.18	−2.10	165.06	77.08	2.30	−2.02	231.02	79.88	2.39	−2.24
145.60	76.36	2.13	−1.89	166.05	77.12	2.33	−2.05	232.05	79.93	2.43	−1.89
145.70	76.36	2.16	−1.55	167.30	77.16	2.31	−2.15	233.25	79.98	2.37	−2.20
145.80	76.37	2.10	−1.93	168.00	77.19	2.29	−2.10	234.01	80.02	2.45	−2.12
145.90	76.37	2.13	−1.93	169.29	77.24	2.30	−1.93	235.55	80.09	2.38	−2.22
146.00	76.37	2.10	−1.97	170.15	77.27	2.28	−2.02	236.53	80.14	2.30	−2.26
146.10	76.38	2.08	−1.93	171.05	77.30	2.27	−2.08	237.12	80.16	2.30	−2.23
146.10	76.38	2.16	−1.98	172.15	77.34	2.30	−1.92	238.05	80.21	2.35	−2.38
146.20	76.38	2.15	−1.94	173.05	77.38	2.42	−1.90	239.21	80.26	2.35	−2.32
146.30	76.39	2.18	−1.83	174.06	77.42	2.26	−1.84	240.14	80.31	2.51	−2.24
146.40	76.39	2.18	−2.08	175.00	77.46	2.23	−1.98	241.00	80.35	2.67	−2.18
146.50	76.39	2.26	−1.77	176.21	77.51	2.26	−1.94	242.14	80.40	2.46	−2.24
146.60	76.40	2.20	−2.16	178.69	77.62	2.25	−1.96	243.16	80.45	2.40	−2.34
146.70	76.40	2.21	−2.07	179.10	77.64	2.20	−2.23	244.00	80.49	2.41	−2.37
146.80	76.40	2.19	−2.02	180.10	77.69	2.27	−2.12	245.06	80.54	2.47	−2.29
146.90	76.41	2.26	−2.14	181.80	77.76	2.33	−2.15	246.18	80.59	2.40	−2.22
147.00	76.41	2.18	−2.44	182.20	77.78	2.34	−2.20	247.10	80.64	2.22	−2.17
147.10	76.42	2.18	−1.97	183.07	77.82	2.31	−2.41	248.15	80.69	2.41	−2.12
147.12	76.42	2.28	−1.86	184.17	77.87	2.40	−2.29	249.10	80.73	2.44	−2.41
147.20	76.42	2.27	−1.81	184.92	77.90	2.24	−1.82	250.16	80.78	2.45	−2.23
147.30	76.42	2.18	−1.97	186.48	77.97	2.27	−1.96	251.19	80.83	2.46	−2.28
147.40	76.43	2.21	−1.84	187.18	78.00	2.40	−2.05	252.20	80.88	2.48	−2.44
147.50	76.43	2.19	−1.90	188.28	78.05	2.44	−1.92	253.00	80.91	2.58	−2.23
147.60	76.43	2.19	−1.68	189.10	78.09	2.44	−2.14	254.09	80.97	2.41	−2.25
147.70	76.44	2.21	−1.79	190.08	78.13	2.40	−1.91	255.12	81.01	2.48	−2.35
148.70	76.47	2.07	−1.72	191.30	78.18	2.69	−1.55	256.17	81.06	2.56	−2.62
148.75	76.48	2.19	−1.85	192.00	78.22	2.50	−1.89	257.08	81.11	2.36	−2.30
148.80	76.48	2.11	−1.67	193.42	78.28	2.45	−2.27	258.18	81.16	2.11	−2.47

Depth (m)	Age (Ma)	δ ¹³ C	δ ¹⁸ O	Depth (m)	Age (Ma)	δ ¹³ C	δ ¹⁸ O	Depth (m)	Age (Ma)	δ ¹³ C	δ ¹⁸ O
259.10	81.20	2.45	−2.29	281.10	82.24	2.44	−2.28	303.35	83.29	2.76	−2.57
260.03	81.25	2.47	−2.23	282.10	82.29	2.60	−2.44	304.10	83.33	2.73	−2.37
261.00	81.29	2.44	−2.25	283.17	82.34	2.33	−2.01	305.00	83.37	2.73	−2.53
262.11	81.34	2.41	−2.24	284.05	82.38	2.50	−2.33	306.05	83.42	2.82	−2.45
263.06	81.39	2.40	−2.48	284.96	82.42	2.58	−2.40	307.01	83.46	2.85	−2.11
264.17	81.44	2.35	−2.38	286.04	82.47	2.54	−2.39	307.90	83.51	2.68	−2.29
265.20	81.49	2.45	−2.40	287.18	82.53	2.54	−2.48	308.00	83.51	2.70	−2.37
266.24	81.54	2.42	−2.92	288.14	82.57	2.54	−2.34	309.00	83.56	2.74	−2.34
267.00	81.57	2.47	−2.46	289.00	82.61	2.50	−2.39	309.90	83.60	2.77	−2.69
268.02	81.62	2.41	−2.47	290.10	82.67	2.67	−2.31	310.11	83.61	2.70	−2.52
269.19	81.68	2.42	−2.55	291.09	82.71	2.63	−2.23	311.28	83.67	2.63	−2.41
270.25	81.73	2.28	−2.38	292.02	82.76	2.63	−2.58	311.90	83.69	2.52	−2.58
271.14	81.77	2.48	−2.59	293.03	82.80	2.67	−2.38	314.90	83.84	2.46	−2.63
272.11	81.82	2.44	−2.62	294.01	82.85	2.52	−2.30	317.90	83.98	2.49	−2.64
273.17	81.87	2.47	−2.65	295.06	82.90	2.66	−2.48	319.90	84.07	2.43	−2.54
274.00	81.91	2.51	−2.44	296.07	82.95	2.65	−2.29	321.90	84.17	2.62	−2.50
275.13	81.96	2.77	−2.54	297.16	83.00	2.73	−2.37	2.74	Data of Jynkyns et al. (1994) and Jarvis et al. (2002) new data		
276.04	82.00	2.51	−1.76	298.12	83.04	2.66	−2.33				
277.05	82.05	2.45	−2.24	299.01	83.09	2.63	−2.46				
278.10	82.10	2.37	−1.70	300.13	83.14	2.77	−2.40				
279.25	82.15	2.55	−2.36	301.21	83.18	2.70	−2.28				
280.11	82.19	2.42	−2.19	302.12	83.23	2.86	−2.41	2.18			

Supplementary Table 3 Age and depth of biostratigraphic and carbon-isotope events used to construct a revised age-model for the Shuqualak-Evans core.

Age Model	Tie points	Age (Ma)	Source
Function 1 (9.45–16.76 m)	1: base <i>Micula prinsii</i> (12.80 m) 2: base <i>Lithraphidites quadratus</i> (16.76 m)	67.30 69.18	Gradstein et al. 2012 Gradstein et al. 2012
Function 2 (16.76–27.43 m)	1: base <i>Lithraphidites quadratus</i> (16.76 m) 2: top <i>Reinhardtites levis</i> (21.34 m)	69.18 70.14	Gradstein et al. 2012 Gradstein et al. 2012
Function 3 (28.96–82.30 m)	1: base CMBE (46.94 m) 2: top <i>Radotruncana calcarata</i> (82.30 m)	73.00 75.71	Voigt et al. 2012 Gradstein et al. 2012
Function 4 (83.82–249.94 m)	1: base <i>Uniplanarius sissinghii</i> (134.11 m) 2: base <i>Broinsonia parca constricta</i> (239.27 m)	77.61 81.38	Gradstein et al. 2012 Gradstein et al. 2012
Function 5 (251.46–253.19 m)	1: presence of <i>Arkhangelskiella cymbiformis</i> (251.97 m) 2: presence of <i>Dicarinella asymetrica</i> (253.19 m)	83.20 83.64	Gradstein et al. 2012 Gradstein et al. 2012